

# Image registration for atlas-based analysis of brain regions in children with craniosynostosis

D.C. Wijnbergen

2021



Universiteit  
Leiden

**TU**Delft Delft  
University of  
Technology

*Erasmus*  
ERASMUS UNIVERSITEIT ROTTERDAM



# Image registration for atlas-based analysis of brain regions in children with craniosynostosis

Diede Wijnbergen

Student number: 4466659

26-07-2021

Thesis in partial fulfilment of the requirements for the joint degree of Master of Science in  
*Technical Medicine*

University Leiden; Delft University of Technology; Erasmus University Rotterdam

Master thesis project (TM30004; 35 ECTS)

Dept. of Biomechanical Engineering, TUDELFT

November 2020 – June 2021

Supervisor(s):

Dr. Esther Bron, Erasmus MC

Prof. dr. Irene Mathijssen, MD, Erasmus MC

Dr. Henri Vrooman, Erasmus MC

Marjolein Dremmen, MD, Erasmus MC

Nine de Planque, MD, Erasmus MC

Thesis committee members:

Prof. dr. ir. Jaap Harlaar, TU Delft (chair)

Dr. Esther Bron, Erasmus MC

Prof. dr. Irene Mathijssen, MD, Erasmus MC

An electronic version of this thesis is available at <http://repository.tudelft.nl/>.



Universiteit  
Leiden

**TU**Delft Delft  
University of  
Technology

*Erasmus*  
ERASMUS UNIVERSITEIT ROTTERDAM



## Acknowledgements

I hereby express my sincere gratitude to all the people who have supported me and have dedicated time to guide me during my master thesis. I would especially like to thank Esther Bron and Henri Vrooman for their weekly supervision. Their insightful feedback and suggestions helped me to improve my methods and lifted my project to a higher level. Through them I was able to improve my skills and learn about many different subjects, such as image registration and deep learning. Additionally, I would like to thank Irene Mathijssen, Marjolein Dremmen and Nine de Planque for their indispensable knowledge and input from a medical point of view. They helped me fully understand the medical problems associated with craniosynostosis and how a technical solution could be used for improving craniosynostosis care. Last but not the least, I would like to thank my family for their constant support and unconditional love.

Diede Wijnbergen  
Delft, The Netherlands  
26-07-2021



# Table of Contents

1	Introduction.....	1
2	Background .....	3
	2.1 MRI Modalities .....	3
	2.2 Brain Atlases .....	4
	2.3 Conventional Image Registration .....	5
	2.4 Learning-Based Image Registration .....	7
3	Methods .....	7
	3.1 Data .....	7
	3.2 Preprocessing .....	10
	3.3 Registration methods .....	14
	3.4 Experiments .....	14
	3.5 Validation and statistics .....	15
4	Results .....	17
	4.1 Quantitative Experiments .....	17
	4.2 Qualitative Experiments .....	17
5	Discussion .....	19
	5.1 Comparison Previous Literature .....	20
	5.2 Limitations .....	20
	5.3 Further Research .....	21
6	Conclusion .....	21
7	Appendices .....	24
	7.1 Appendix A — Synthetic Data .....	24
	7.2 Appendix B — Brain Areas .....	25
	7.3 Appendix C — VoxelMorph Optimization Synthetic Data .....	28
	7.4 Appendix D — VoxelMorph Optimization Craniosynostosis Data .....	30
	7.5 Appendix E — Elastix Registration Synthetic Data .....	32
	7.6 Appendix F — Elastix Registration Craniosynostosis Data .....	37
	7.7 Appendix G — VoxelMorph Registration Synthetic Data .....	42
	7.8 Appendix H — VoxelMorph Registration Craniosynostosis Data .....	47



# Image Registration for Atlas-based Analysis of Brain Regions in Children with Craniosynostosis

Diede C. Wijnbergen<sup>1,2,3</sup>, Henri A. Vrooman<sup>1</sup>, Catherine A. de Planque<sup>2</sup>,  
Marjolein H.G. Dremmen<sup>1</sup>, Irene M.J. Mathijssen<sup>2</sup>, and Esther E. Bron<sup>1</sup>

<sup>1</sup> Radiology & Nuclear Medicine, Erasmus MC, Rotterdam, Netherlands

<sup>2</sup> Plastic and Reconstructive Surgery, Erasmus MC, Rotterdam, Netherlands

<sup>3</sup> Technical University Delft, Delft, Netherlands

**Abstract.** To optimize treatment in patients with craniosynostosis, better understanding of the disease process is essential, for example using brain MRI analysis to study brain volume, brain perfusion, and brain micro-architecture. However, such analyses require image registration, which is challenging because of disease-related brain deformations. Therefore, the aim of this project is to optimize image registration for children with syndromic craniosynostosis, aged 0 to 6 years old. We compared conventional and deep learning registration methods in a quantitative evaluation using synthetic data (i.e. deformed atlases) and in a qualitative experiment using registration of atlas scans to craniosynostosis scans. In addition to comparing registration methods, we evaluate the influence of using both T1-weighted and T2-weighted scans and using an infant or adult atlas. Our qualitative results showed that head shape was registered well by both the conventional and the deep learning registration method, while the deep learning method performed better regarding registration of the ventricles. Quantitatively, our results showed that white matter structures were registered well (Dice: 0.70-0.81). However, regarding registration of the cortical brain regions, both methods resulted in a sub-optimal accuracy (Dice: 0.45-0.63). In general, the approaches of using T2-weighted infant atlases or T1-weighted adult atlases outperformed the alternative approaches. In conclusion, we obtained the best registration result using the deep learning approach, probably as prior spatial information is incorporated in the training process. In addition, we showed that infant atlases based on T2-weighted scans lead to the best results in registration of infant scans.

**Keywords:** Image Registration · Craniosynostosis · Deep Learning

## 1 Introduction

Craniosynostosis is a congenital disorder in which one or more cranial sutures close prematurely, causing skull, brain, and facial anomalies [1]. The prevalence of this disorder is currently 7.2 in 10.000 live births for the Netherlands [2]. Craniosynostosis is often accompanied by an increased risk in behavioural disorders, neurocognitive problems and brain abnormalities such as ventriculomegaly,

especially in severe cases of syndromic or multisuture craniosynostosis [1, 3]. Currently, treatment is directed at preserving intracranial pressure and restoring the shape of the head by surgery within the first year of life [1, 3]. However, it is yet unclear which patients benefit from surgery, as it is unknown which functional and structural brain abnormalities relate to growth restriction of the skull [4, 5].

To optimize treatment, it is necessary to improve understanding of the implications of craniosynostosis on the developing brain. A key step is studying the impact of the disease on brain structure and function using advanced magnetic resonance imaging (MRI) techniques such as high resolution structural MRI, arterial spin labelling and diffusion tensor imaging. This requires image registration, for example to align the brain with an existing brain atlas for identification of brain regions [6]. However, registration of MRI scans of children with craniosynostosis is challenging. First, in young children, the brain is still growing and the contrast between grey and white matter is constantly changing due to the ongoing myelination [7–9], which complicates registration of the cortex. Second, standard registration methods may be unable to compensate for the severe brain and skull deformations.

In recent years, image registration methods increasingly use deep learning [10], which has shown to be faster and overall has a better performance than conventional registration methods [11, 12]. However, neither conventional nor deep learning registration methods have been previously applied to MRI scans of brains with large deformations. Therefore it is unknown if deep learning methods also outperform conventional registration methods when registering scans with large deformations such as seen in craniosynostosis. Considering brain growth and changing contrasts, both T1-weighted (T1w) and T2-weighted (T2w) scans have been shown added value for brain segmentation [13]. This is due to the fact that the contrast between white matter (WM) and gray matter (GM) is better visible on T2w scans before an age of 6 months, while it is better visible on T1w scans after an approximate age of 9 months. Using both T1w and T2w scans may improve registration, as this would allow for the use of information from either modality at each developmental stage. Additionally, the use of either an infant or adult brain atlas could also influence the registration performance, as young infants display a distinctively different WM-GM pattern than older infants and children [8]. While no research has been performed on any of these aspects, it is necessary to evaluate how current registration methods perform on craniosynostosis brain imaging data and how these methods might be improved to include brain growth, changing contrasts and brain deformations using different scan modalities and atlases.

This work aims to evaluate conventional and deep learning methods for registration of brain atlases in children with syndromic craniosynostosis, aged 0 to 6 years old. We will perform quantitative experiments on deformed atlas data and qualitative experiments on data of patients with craniosynostosis. Additionally, we will evaluate the influence of using both T1w and T2w scans and using an infant or adult atlas.

## 2 Background

### 2.1 MRI Modalities

T1w and T2w images are two of the most commonly used structural MRI sequences [14], on which tissues show different intensities due to differences in T1 and T2 tissue relaxation times [14]. On T1w scans, tissues with a high lipid content show a high intensity (fat, brain white matter) and other areas show a lower intensity (air, spinal cord, cerebrospinal fluid (CSF), grey matter). On T2w scans tissues with a high water content show a high intensity, such as the CSF. An example of T1w and T2w brain MRI scans is shown in Figure 1.

T1w and T2w sequences can be used to study the developing infant brain, especially regarding the process of myelination [14, 15]. Myelination of brain regions starts during the fifth fetal month and proceeds up to about 2 years of age [15]. Since myelin consists of 70 percent lipids [14], white matter changes from a darker than grey matter intensity to a very bright intensity on the T1w scan during myelination [16]. This causes a shift in intensities in both T1w and T2w images as can be seen in Figure 1 [9]. As myelination continues, white and grey matter are better distinguished on T2w weighted images until an approximate age of six months is reached [8, 17]. Between six and nine months of age, contrast between white and grey matter is low on both the T1w and T2w scans [8, 17]. After an approximate age of nine months, white and grey matter are better distinguished on T1w weighted images [8, 17]. Therefore, it could be useful to use both T1w and T2w scans for registration of brain atlases to brain scans of infants and children with craniosynostosis.

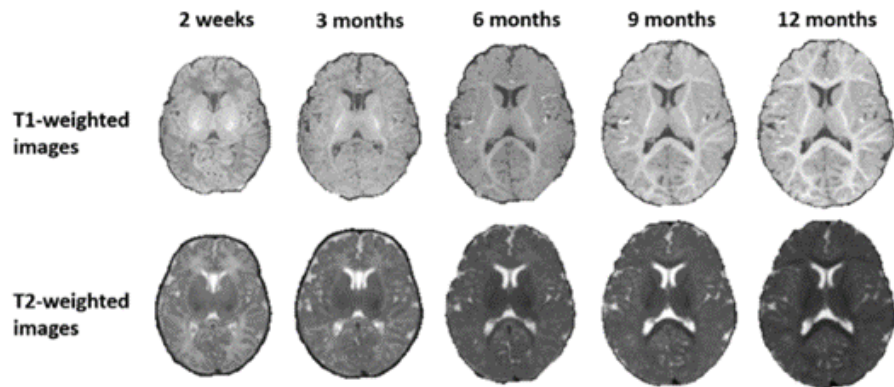


**Fig. 1.** Registered T1-weighted (T1w) and T2-weighted (T2w) MRI images of an infant, longitudinally scanned at 2 weeks, 3, 6, 9 and 12 months of age [17].

## 2.2 Brain Atlases

A brain atlas consists of one or multiple reference scans (e.g. T1w/T2w), each containing a set of labels belonging to the different brain regions, as can be seen in Figure 2. The atlas represents a brain with certain characteristics, such as a certain age. The atlas scan and corresponding labels can be registered to a patient image to obtain the labels for the individual patient [18].

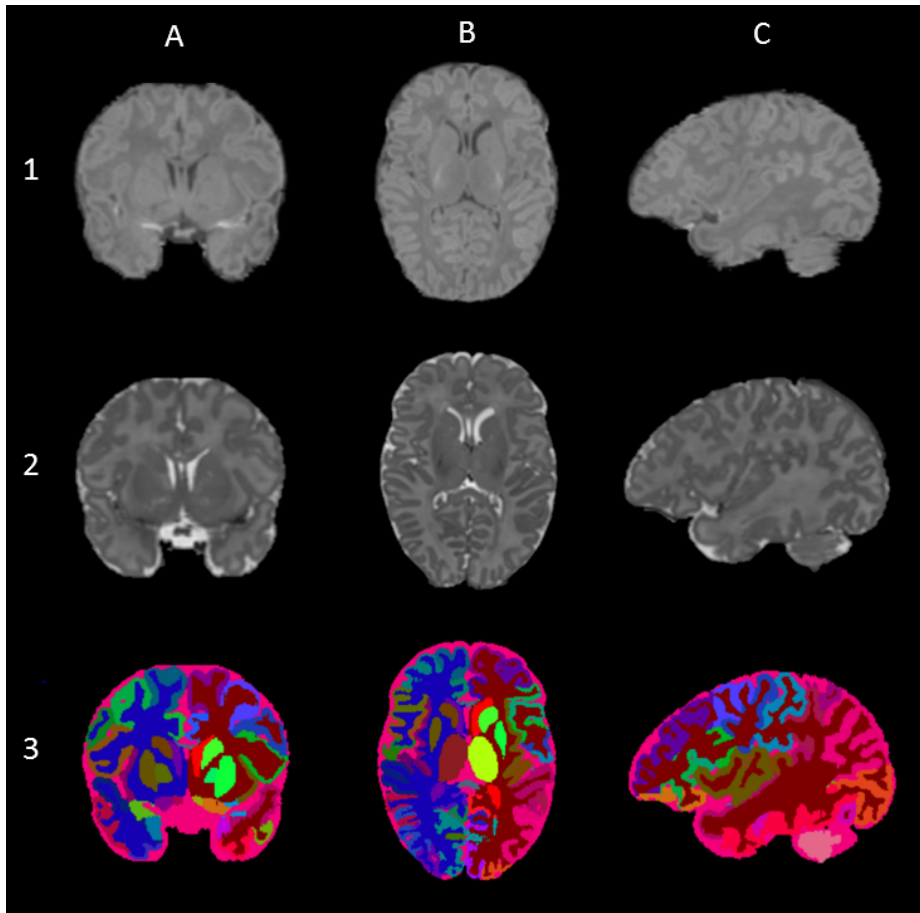


**Fig. 2.** M-CRIB infant brain atlas with 100 different labels, T1-weighted images (1), T2-weighted images (2) and atlas images (3) are shown in coronal (A), axial (B) and sagittal (C) plane [19].

Many adult brain atlases are available for atlas-based image registration; however, the availability of infant brain atlases is limited due to difficulty in manual segmentation [18, 20]. This is mostly caused by low tissue contrast, high

image noise and movement artefacts [18, 20]. An atlas containing both T1w, T2w scans and a detailed parcellation map at different time points between the ages of 0 and 2 years is preferable. However, such an atlas is still missing. Also, no atlases are yet available that take any pathological cases into consideration. Therefore, in the current study, atlases of ten healthy infants and ten healthy adults are used. The atlases are further described in the methods section.

### 2.3 Conventional Image Registration

Image registration concerns the alignment of a moving image  $I_M$  to a fixed image  $I_F$  by a transformation  $T$ . The objective of image registration is estimating the optimal transformation by minimizing the dissimilarity  $C$  between  $I_F$  and the transformed  $I_M$ :

$$T = \operatorname{argmin}_T C(I_F, T(I_M)) \quad (1)$$

Conventional registration methods solve an optimization problem on a pair of images, where each pair is solved independently. Differences in conventional registration methods are mostly based on four different components: the image features, the dissimilarity measure, the transformation model and the optimization used for the registration [21, 22].

- **Images features:** Dissimilarity  $C$  is a metric, calculated based on certain image features. Image features are most often the voxel intensities, but can also be gradient magnitudes, edges, curves, landmarks or Gabor filters.
- **Dissimilarity measure:** The dissimilarity measure is the metric which is used to calculate the dissimilarity  $C$ . Several examples are: Sum of squared distances (SSD), sum of absolute distances (SAD), mean squared distance (MSD), (normalised) cross-correlation (NCC/CC), correlation ratio (CR) and (normalised) mutual information (NMI/MI).
- **Transformation model:** The transformation model determines which transformation parameters are optimized. Transformation models can be divided into rigid transformations: translation and rotation. And non-rigid transformations: scaling, shearing, affine (includes translation, rotation, shearing and affine) and B-Spline deformation. A rigid or affine transformation step often precedes a non-rigid B-spline registration. A few examples of transformation models are shown in Figure 3.
- **Optimization method:** The optimization method is the way in which the optimal transformation parameters are determined, for which  $C$  is minimized. Several examples are: gradient descent, adaptive stochastic gradient descent, Newton/Levenberg-Marquardt and Gaussian-Newton.

Finding the optimal transformation is an iterative process in which during each step, image dissimilarity is determined based on the image features. Then  $I_M$  is transformed according to the transformation model, for which the image dissimilarity is minimized. This iterative process is continued until a measure is

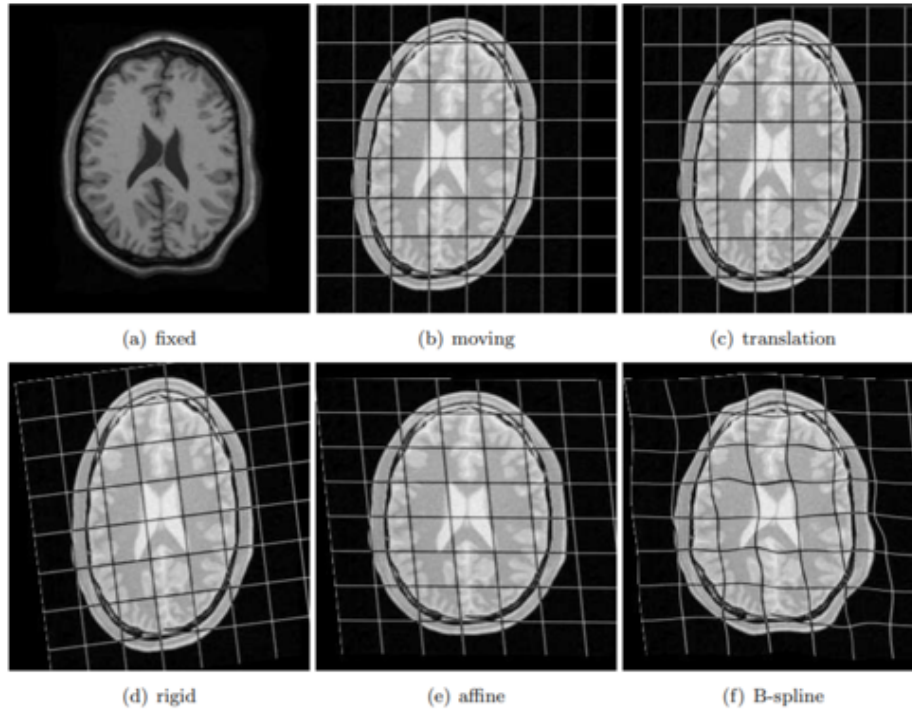


**Fig. 3.** Several different transformation models. Fixed image (A), moving image (B), translation (C), rigid deformation (D), affine deformation (E) and B-Spline deformation (F) [23].

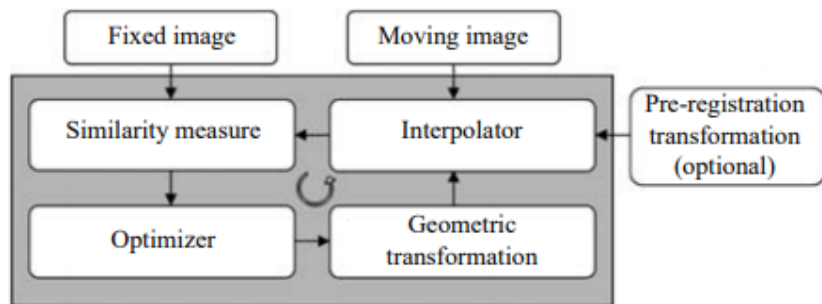


**Fig. 4.** Typical algorithms used in intensity-based registration methodologies [21].

satisfied or until a maximum number of iterations is reached. A typical algorithm used in registration is shown in Figure 4.

Apart from the four mentioned components, Eq. 1 is often extended by adding a regularization factor  $\text{reg}(T)$ , which ensures smoothness of the estimated deformation field and prevents an optimization to local minima. The regularization parameter  $\lambda$  determines the degree of smoothness. Thus, the formula becomes:

$$T = \underset{T}{\text{argmin}} C(I_F, T(I_M)) + \lambda \text{reg}(T) \quad (2)$$

Furthermore, an interpolator is used to resample the voxel intensity of the moving image into the new coordinate system [21]. In addition, in many registration methods a multi-resolution approach is used, in which image registration is performed from lower to higher resolution images [21]. More elaborate reviews on conventional registration methods are available [21, 22].

## 2.4 Learning-Based Image Registration

Learning-based image registration directly evaluates a function that maps an input image pair to a deformation field. Instead of registering a single pair of images using conventional optimization techniques, learning-based methods perform global optimization of shared parameters of a large set of image pairs. A global registration function is learned from training data, and then applied onto pairs of images to perform registration. [11]

Image registration using deep learning optimizes the same equation as stated in Eq. 2, as the equation is used as loss function in the neural network. The inputs to the network are certain image features (voxel intensities), on which a dissimilarity measure is determined. However, the optimization of the transformation parameters is now done by a neural network. Once trained, the learning-based image registration methods have a higher accuracy and execute the registration faster [11, 12].

The structures of both the conventional and deep learning registration methods used in the current study are further described in the methods section.

## 3 Methods

### 3.1 Data

For evaluating the conventional and deep learning registration methods, the following atlases, synthetic datasets and craniosynostosis dataset were used.

**Atlases** Atlases of ten healthy infants and ten healthy adults were used. The parcellations of ten healthy infants are included in the M-CRIB Atlas 2.0 created by Alexander et al. [19]. This atlas contains the T1w and T2w MRI scans, and manual segmentations of 100 brain regions for each infant. Segmentations of the brain regions were based on the Desikan-Killiany adult cortical atlas, to ensure

compatibility with FreeSurfer [24]. The parcellations of the adult atlases were obtained by processing the T1w and T2w MRI scans of ten healthy adults participating in the Rotterdam Study [25]. These participants were processed using FreeSurfer, making them compatible with the M-CRIB Atlas 2.0. An example of T1w and T2w images of both infant and adult atlases, with corresponding parcellations are shown in Figure 5.

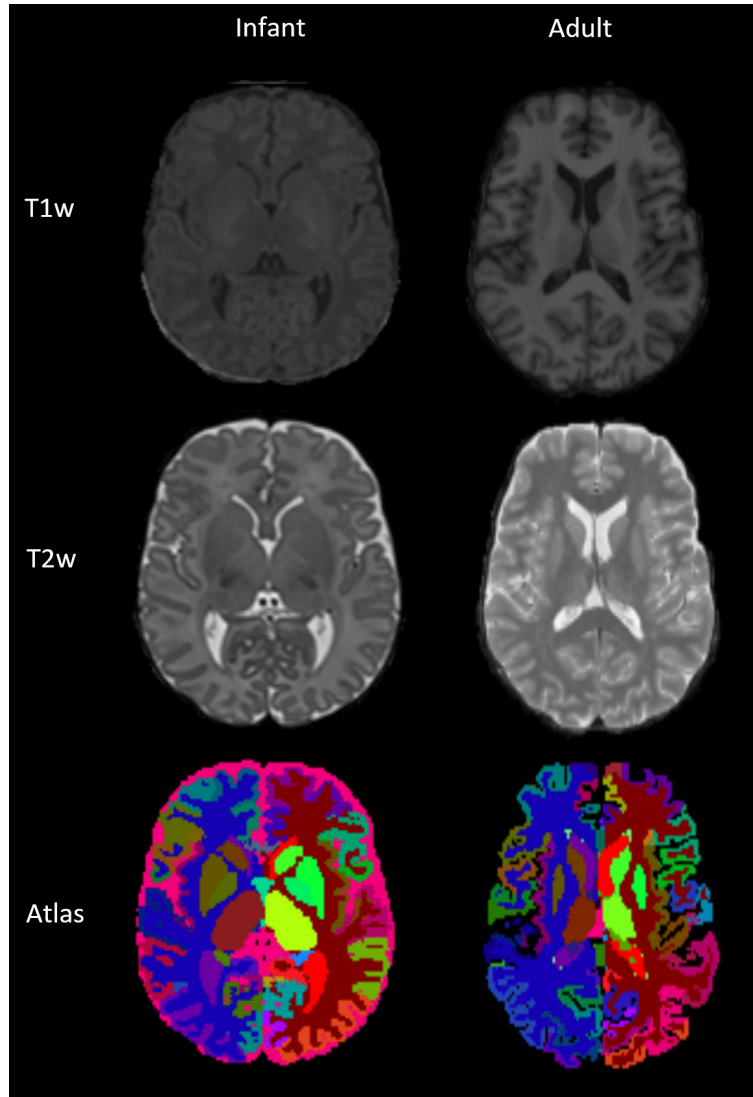


**Fig. 5.** T1w images, T2w images and atlas of infant and adult atlas.

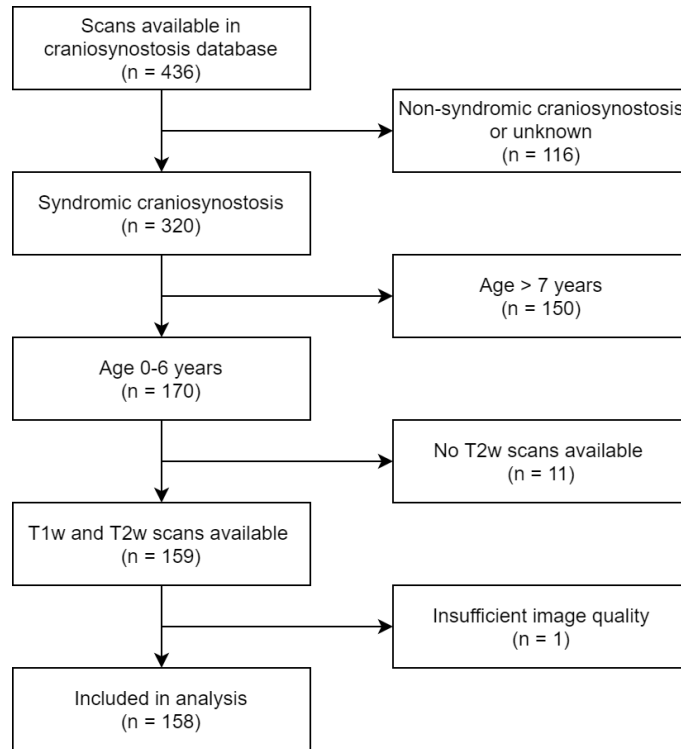


**Fig. 6.** Flowchart of the inclusion of patients with syndromic craniosynostosis, aged 0-6 years old.

**Table 1.** Characteristics of included patients.

Grouping	MRIs	Unique patients
Male, n (%)	84 (53.2)	60 (49.6)
Female, n (%)	74 (46.8)	61 (50.4)
Apert, n (%)	27 (17.1)	18 (14.9)
Crouzon, n (%)	45 (28.5)	27 (22.3)
Muenke, n (%)	20 (12.7)	17 (14.0)
Pfeiffer, n (%)	7 (4.4)	4 (3.3)
Saerthre-Chotzen, n (%)	18 (11.4)	14 (11.6)
Complex, n (%)	36 (22.8)	30 (24.8)
Tcf12, n (%)	5 (3.2)	5 (4.1)
Mean age at scan, yrs (std)	2.5 (1.85)	-
Total MRIs	158	121

**Synthetic Data** To evaluate the performance of the registration methods against a ground-truth, we created two synthetic datasets by non-rigidly deforming the infant and adult atlases. The non-rigid deformation was generated using a normalized random displacement field, in which for each voxel a 3D displacement vector  $\mathbf{u}$  was created with random values between -0.5 and 0.5 [26]. The magnitude of the displacement in the deformation field is determined by multiplying the vectors with the parameter  $\alpha$ (Eq. 1) [26]. Here,  $R_o$  and  $R_w$  describe the location of the voxels in the original and warped images respectively.

$$R_w = R_o + \alpha \mathbf{u} \quad (3)$$

Subsequently, the displacement field is smoothed using a Gaussian filter, in which the standard deviation of the kernel is determined by the parameter  $\sigma$ . Therefore,  $\sigma$  determines the smoothness of the deformation field [26]. For creating the synthetic data sets, values of  $\alpha$  were randomly chosen between 1200 and 1600, and values of  $\sigma$  were randomly chosen between 7 and 10. These values were chosen to imitate deformations caused by craniosynostosis as closely as possible. Examples of atlas scans deformed with different combinations of  $\alpha$  and  $\sigma$  are shown in Appendix A. 30 synthetic scans were created for each individual adult and infant atlas, resulting in a total of 300 synthetic scans for the infant atlas and 300 for the adult atlas.

**Craniosynostosis Data** We considered all children between the ages 0 and 6 with syndromic craniosynostosis (Apert, Crouzon-Pfeiffer, Muenke, Saethre-Chotzen, TCF12, complex) that had MRI data acquired at the Dutch Craniofacial Center (Erasmus University Medical Center) between 2008 and 2019 for inclusion. For complex craniosynostosis, a genetic cause is unknown, but expected because multiple sutures are involved. Patients were scanned on a 1.5T scanner (GE Healthcare, either Signa HDxt or Signa Explorer). Patients were included if both 3D T1w and T2w scans were available. A flowchart of the inclusion of the craniosynostosis MRI data is shown in Figure 6. We included 158 scans from 121 unique patients. One subject was excluded due to insufficient image quality. Patient characteristics are shown in Table 1.

### 3.2 Preprocessing

The preprocessing pipelines used for the atlases and craniosynostosis data are visualised in Figure 7. Each preprocessing step is explained in more detail in the following sections. The synthetic data was created using the fully preprocessed atlases. Images resulting from each preprocessing step are shown in Figure 8.

**N4ITK Bias Correction** Each T1w and T2w image was corrected for intensity non-uniformity using the N4ITK algorithm [27]. The following settings were used for the correction; an initial mesh resolution of 200, a number of four times 50 iterations and a convergence threshold of  $1 \cdot 10^{-10}$ .

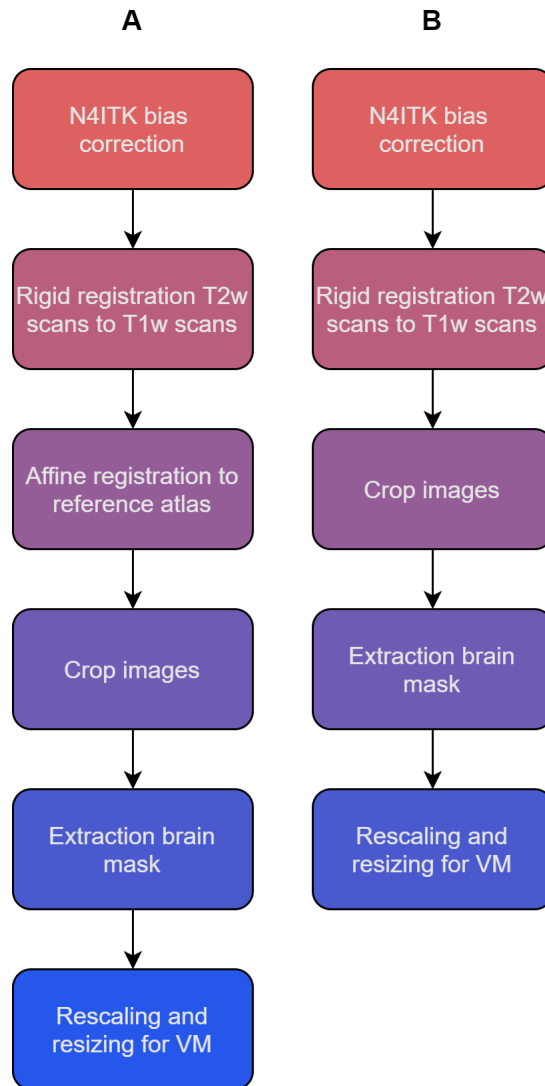


**Fig. 7.** Pipelines for the preprocessing of atlases (A) and craniosynostosis data (B). VM = VoxelMorph.

**T2w to T1w Image Registration** For each patient and atlas, the T2w scan was rigidly registered to the T1w scan using Elastix. Often, the T2w scan contained a large part of the neck, in addition to the head. By registering the T2w scan to the T1w scan, the T2w scan was automatically cropped to fit on the T1w scan. This eliminated the need for further removal of the neck from the scans to ensure correct brain extraction in a later preprocessing step. For the rigid registration, a normalized mutual information (NMI) similarity metric and an adaptive stochastic gradient descent optimization method were used.

**Affine Registration to Reference** This preprocessing step was only executed for the atlases. For both the infant and adult atlas, one atlas was chosen as a reference to affinely register all other atlases to. Aligning all atlases to a reference ensured that there were only non-rigid deformations present in the synthetic datasets. Therefore, it was unnecessary to perform affine registration before evaluating the registration methods on the synthetic data. For the affine registration, a NMI similarity metric and an adaptive stochastic gradient descent optimization method were used.

**Crop Images** After registering the images, all T2w scans were cropped as much as possible to remove the empty space around the skull. This was accomplished using the crop image function available in the nilearn Python toolbox [28]. For cropping, a relative tolerance of 0.1 was used. The offsets, with which the T2w scans were cropped, were then applied to the T1w scans and parcellation maps.

**Brain Extraction** For both registration methods, skull-stripped atlases and craniosynostosis scans were used. These skull-stripped images were acquired by extracting the brain using the Brain Extraction Tool (BET) from the FMRIB Software Library (FSL) [29]. A fractional intensity threshold of 0.3 was used, ensuring extraction of the whole brain. Additionally, the robust brain centre estimation option was used. This option repeatedly calls BET up to a maximum of 10 iterations, each time setting the starting centre of the brain estimation to the centre-of-gravity of the previously estimated brain extraction. The iterations stop when the centre-of-gravity stops moving.

**Rescaling and Resizing** For using the atlases and craniosynostosis data in VoxelMorph, the scans needed to be rescaled between the values 0 and 1. After rescaling, the skull-stripped images were further cropped by determining the most inferior point of the extracted brain. This point was then used to remove the remaining empty space beneath the brain, which was created by skull-stripping a.o. the neck using BET in the previous preprocessing step. Then, the images were resized to a size of 128 x 128 x 128. Additionally, to prevent the GPU from running out of memory during training, the data type of the images was set from float32 to float16.

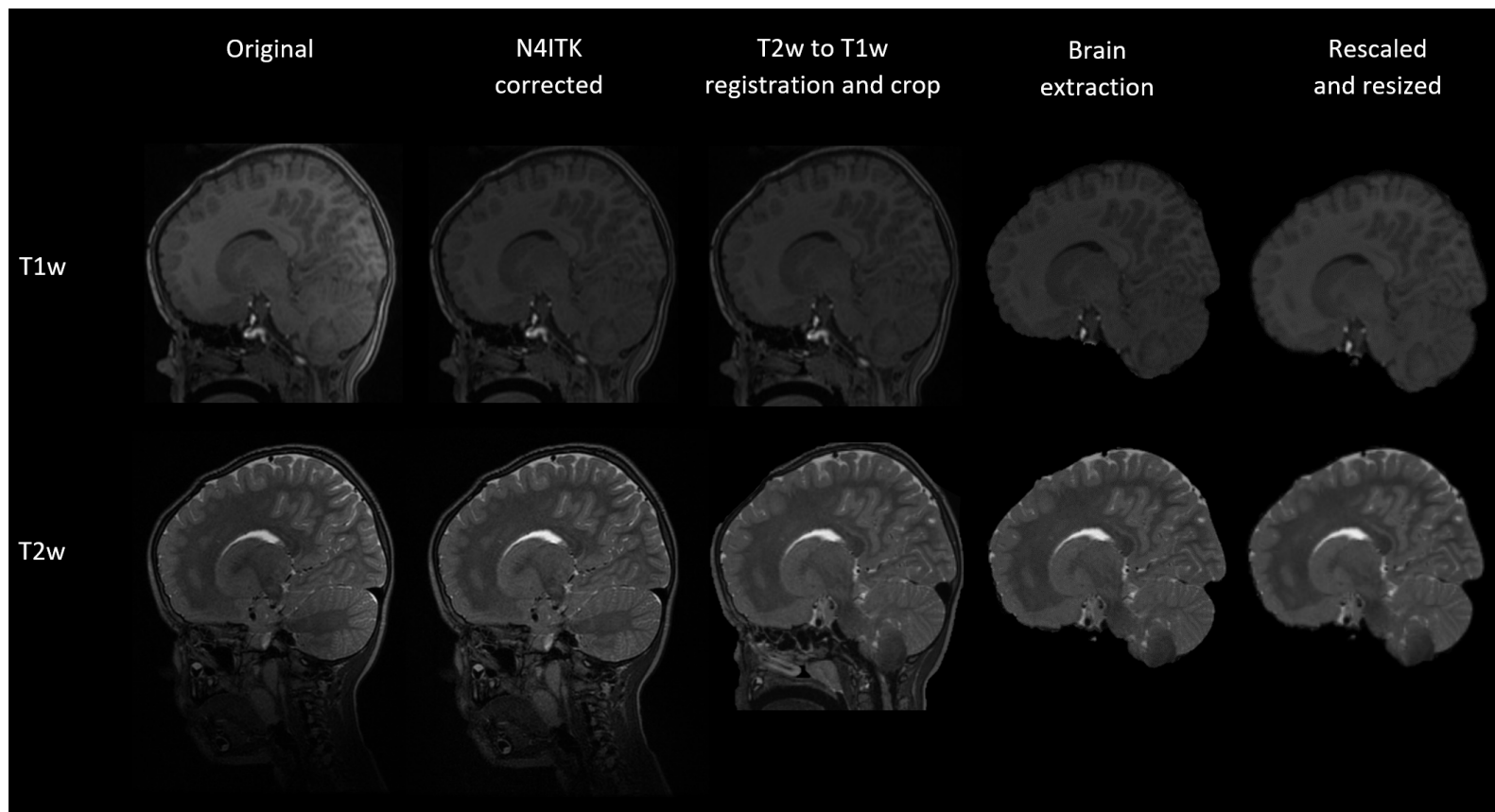


**Fig. 8.** Preprocessing steps performed on a patient with craniosynostosis, shown on both T1w and T2w images. The step involving the affine registration to a reference scan is not shown.

### 3.3 Registration methods

**Conventional Registration** As conventional registration method, we used Elastix which is a toolbox for rigid and non-rigid image registration that uses free-form deformations (FFD) based on the parameters of a cubic B-spline function [23]. These parameters were optimized using adaptive stochastic gradient descent optimization with a normalized mutual information (NMI) similarity metric. Furthermore, a pyramid scheme using three different resolutions (with downsampling factors four, two and one) was used, executing the registration from a coarse to fine image resolution.

**Deep Learning-based Registration** As deep learning registration method, the VoxelMorph neural network was used [11]. VoxelMorph is an unsupervised network that directly evaluates a function that maps an input image pair to a deformation field. The network parameters/CNN kernels of VoxelMorph were optimized using the NMI similarity metric and the ADAM optimizer with a learning rate of  $10^{-4}$ . Due to the size of the data, a batch size of 1 was used. The network was trained using a number of 1500 epochs, a masked loss, a regularization parameter of 0.2 for the quantitative experiments and a regularization parameter of 0.8 for the qualitative evaluation. Optimization of these parameters is shown in Appendix C and D. Training, validating and testing of the network were all executed using a GeForce RTX 2080 Ti.

### 3.4 Experiments

**Quantitative Experiments** Quantitative experiments were performed using the synthetic data. Each original atlas was registered to each deformed synthetic scans to evaluate the performance of both registration methods against a ground-truth. Registrations were performed for all combinations of image modalities (T1w, T2w, or combination of T1w and T2w) and atlases (infant or adult) as input. For the deep learning-based registration, the VoxelMorph network was trained, evaluated and tested for each of these six input combinations. Registration accuracy is here quantified as the overlap of brain regions, determined using the Dice score. An overview of the division of brain labels into brain regions is shown in Appendix B.

**Qualitative Experiments** Qualitative experiments were performed using the craniosynostosis dataset. Each infant and adult atlas was registered to each craniosynostosis patient. Registrations were performed for all combinations of image modalities (T1w, T2w, or combination of T1w and T2w) and atlases (infant or adult) as input. Registration performance was evaluated visually. The visual evaluation mostly focused on the head shape, ventricle shape and the grey matter pattern of the deformed atlas. We scored a brain to have normal or abnormal structure based on the head shape and the presence of ventriculomegaly into four categories: 1) age < 6 months with normal brain structure, 2) age < 6 months

with abnormal brain structure, 3) age > 2 years with normal brain structure, and 4) age > 2 years with abnormal brain structure.

### 3.5 Validation and statistics

**Data Set Split** Both synthetic datasets were divided into 200 scans for training, 50 for validation and 50 for testing for VoxelMorph. The test set was also used for evaluation of Elastix. The craniosynostosis dataset was divided on a patient level into 126 scans (80% of patients) for training, 14 scans (10% of patients) for validation and 18 scans (10% patients) for testing.

**Dice-score** Registration accuracy is quantified as the overlap of brain regions between the synthetic atlas and the registered atlas in ten cortical and subcortical areas using Dice score:

$$Dice(X, Y) = \frac{2 * |X \cap Y|}{|X| + |Y|} \quad (4)$$

**Statistics** Differences in Dice scores were tested by paired two-sided t-tests. Comparisons were made between all combinations of input and registration methods (6 tests), the image modalities (12 tests) and the atlases (6 tests) per brain region. The Bonferroni method was conducted to correct for multiple comparisons. Values of  $p < 2.10e^{-3}$  were considered statistical significant ( $\alpha = 0.05/24$ ).

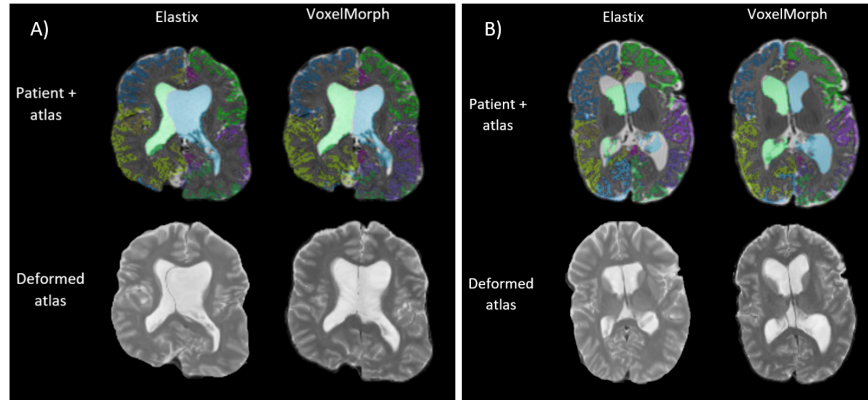


**Fig. 9.** T2w images of an adult atlas registered to a child with craniosynostosis using Elastix. A) Registration was performed using T1w images. The brain pattern of this child is relatively old and abnormal looking. B) Registration was performed using T2w images. The brain pattern of this child is relatively young and abnormal looking.

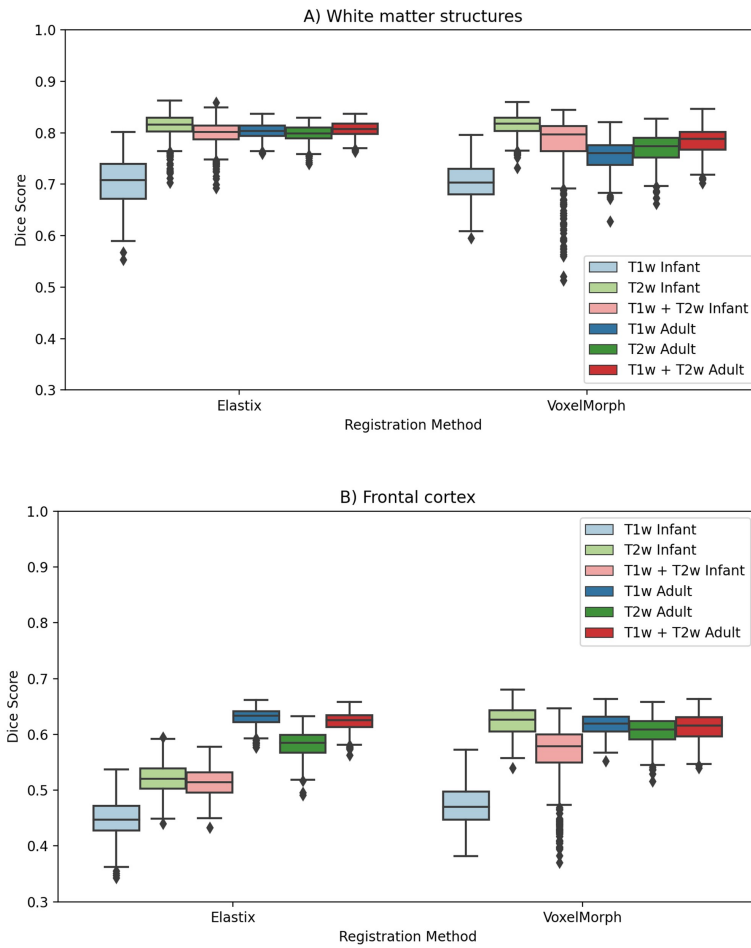


**Fig. 10.** Boxplots of the Dice scores for the registration of infant and adult atlases to the synthetic datasets. Only results for the white matter structures (A) and frontal cortex (B) are shown, as other white matter and cortex regions showed comparable results.

## 4 Results

### 4.1 Quantitative Experiments

Figure 10 shows the registration accuracy for the synthetic data experiments. Regarding registration methods, both Elastix and Voxelmorph significantly outperformed the other method in some settings. The most significant difference was observed in registering the frontal cortex using T2w infant scans with Elastix (Dice = 0.52) and VoxelMorph (Dice = 0.62,  $p < 0.0001$ ). Regarding image modalities, T1w scans (Dice = 0.63) and the combination of T1w and T2w scans (Dice = 0.62) of the adult atlas yielded significantly higher performance than T2w scans (Dice = 0.58,  $p < 0.0001$ ). However, for the infant atlas, registration accuracy using T2w scans (Dice = 0.62) was significantly higher than when using only the T1w scans (Dice = 0.48,  $p < 0.0001$ ). Regarding atlases, both infant and adult atlases showed high performances. The most significant difference between the infant atlas (Dice = 0.45) and the adult atlas (Dice = 0.63) could be observed when using T1w scans for registration of the frontal cortex ( $p < 0.0001$ ).

### 4.2 Qualitative Experiments

Overall, visual evaluation showed similar results for all registration settings regarding the head shape and the grey matter pattern. However, when evaluating the ventricles, Elastix registration in some cases resulted in a mid-line shift of the ventricles. This happened for 14.4% of the craniosynostosis scans with a relatively abnormal looking brain, both young and old, and for different types of input modalities and atlases. An example of the mid-line shift is shown in Figure 10A. VoxelMorph did not result in any mid-line shifts. Additionally, VoxelMorph showed better registration of the ventricles in craniosynostosis scans with a relatively abnormal brain (see example in Figure 10B).

Regarding imaging modalities, the use of T2w scans or the combination of T1w and T2w scans of infant atlas resulted in better registration of the brain outline than when using T1w scans (Figure 11). Similarly, for the adult atlases, using T1w scans or the combination of T1w and T2w scans resulted in a better registration of the brain outline (Figure 12), which is in line with the results shown for the synthetic data. Additionally, the use of both T1w and T2w led to less cases with ventricle mid-line shift. Regarding the type of atlas, in some cases using the infant atlas resulted in a better overlap (Figure 13, red circles) and in some cases the adult atlas did (yellow circles). Both types of atlases did not show perfect overlap with the craniosynostosis grey matter patterns. However, when registering the brain of a relatively young patient, the infant atlas showed better overlap of the ventricles and white matter than the adult atlas.

An elaborate overview of all results is shown in Appendix E (Elastix registration on synthetic data), Appendix F (Elastix registration on craniosynostosis data), Appendix G (VoxelMorph registration on synthetic data) and Appendix H (VoxelMorph registration on craniosynostosis data).

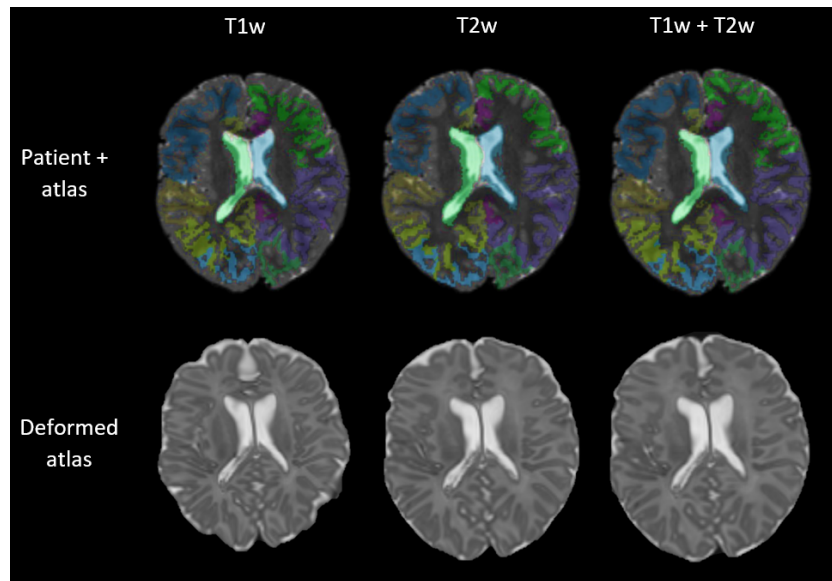


**Fig. 11.** T2w images of an infant atlas registered with Elastix to the scans of a child with a relatively old and normal appearing brain.

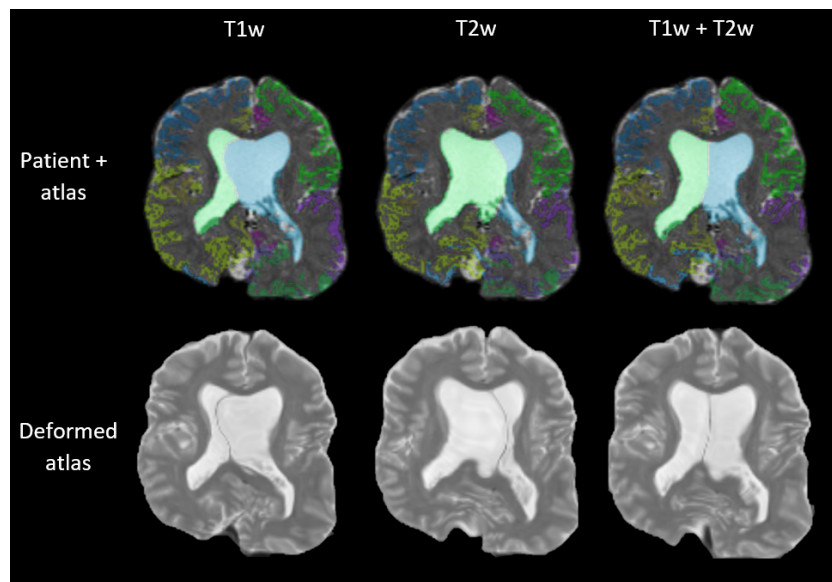


**Fig. 12.** T2w images of an adult atlas registered with Elastix to the scans of a child with a relatively old and normal appearing brain.

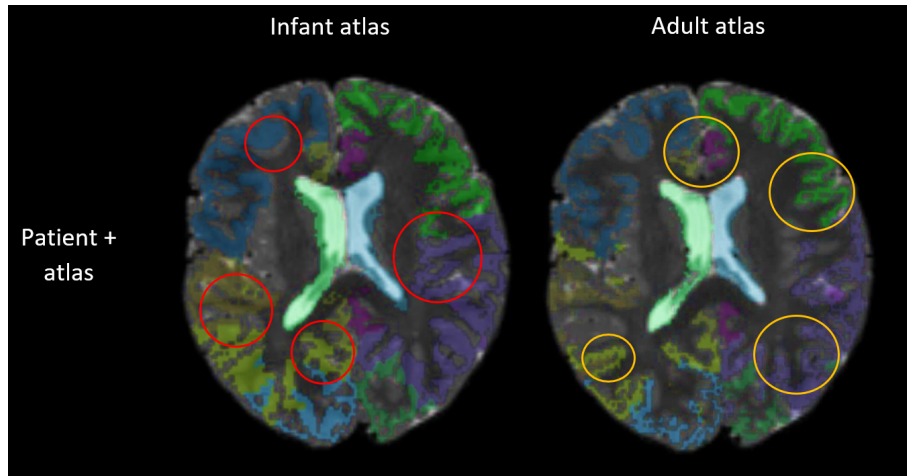


**Fig. 13.** T2w images of an infant and adult atlas registered to a child with craniosynostosis using Elastix. Registration was performed using the combination of T1w and T2w images. Regions where the infant atlas results in a better grey matter overlap are displayed with red circles, regions where the adult atlas does are displayed with yellow circles. The brain pattern of this child is relatively old and normal looking.

## 5 Discussion

In the current study, we evaluated the performance of conventional and deep learning registration methods on the registration of brain atlas MRI scans to brain MRI scans of children with syndromic craniosynostosis. VoxelMorph resulted better registration of cortical brain regions than Elastix in synthetically deformed infant scans. Furthermore, the best registration results were obtained when using T2w scans for infant synthetic data and T1w scans or the combination of T1w and T2w scans for adult synthetic data. This confirms the hypothesis that using T2w scans might be beneficial when registering infant MRI scans. Additionally, in the frontal cortex, adult synthetic data yielded significantly higher Dice scores than infant synthetic data, confirming the difficulty associated with registering and segmenting grey matter in infant scans.

Visual inspection showed better registration of craniosynostosis data using VoxelMorph than using Elastix. In particular regarding registration of the ventricles, as Elastix occasionally caused a mid-line shift or incomplete registration of the ventricles. Such registration faults did not occur when using VoxelMorph as prior information was obtained during training of the neural network, which was then applied to each scan. This implies that registration of deformed scans is more easily optimized using a neural network instead of pair-wise registrations. In accordance with the quantitative evaluation, the brain outline was better registered using the T2w scans for registration using infant atlases and using the T1w scans for registration using adult atlases. However, regarding registration

of the cortical brain regions, both Elastix and VoxelMorph methods resulted in a sub-optimal overlap using either the infant or adult atlas.

### 5.1 Comparison Previous Literature

Neither conventional nor deep learning registration methods have been previously applied to MRI scans of brains with large deformations. Therefore, it is not possible to directly compare the results of this study to previous literature. However, in comparison to adult brain registration using different conventional registration methods, similar results were found by Klein et al. [30]. When registration was performed using brains scans with a similar number of parcellations as used in the current study, Dice scores around 0.5 were reached [30] for the cortical brain regions. Dice scores of cortical brain regions in the current study ranged from 0.45 to 0.63, slightly higher than results by Klein et al. [30], most probably as Dice scores were computed on synthetic data. Balakrishnan et al. [11] obtained Dice scores of around 0.7-0.8 for registration of white matter structures using the learning-based registration method, which is comparable to the Dice scores ranging between 0.70 and 0.81 for learning-based registration of white matter structures obtained in the current study. Dice scores of other brain regions could not be compared as Dice scores by Balakrishnan et al. [11] were computed on larger parcellations than in the current study. For registration of atlas MRI scans to MRI scans of children with craniosynostosis the learning-based method outperformed the conventional registration method, as it was able to learn spatial prior information in the training process. This corresponds with previous literature, as deep learning methods were found to have a faster and overall better performance than conventional registration methods [11, 12]. Additionally, just as using T2w scans in addition to T1w scans has shown added value for brain segmentation [13], using the T2w scans has also shown added value for brain registration in children with craniosynostosis.

### 5.2 Limitations

A main limitation of this study is that no ground-truth labels were available and therefore Dice scores were computed on synthetic datasets only. Instead, qualitative evaluation was used for evaluation of the registration of craniosynostosis scans. Qualitative evaluation is subjective and does not allow for statistic testing between different methods. However, the use of Dice scores is also limited as these scores highly depend on the size of the brain area that is registered. Therefore, Dice scores between different brain areas cannot be compared. Furthermore, although MRI-scans from a diverse group of craniosynostosis patients were used, the scans were all derived from the same medical centre and no external dataset was used to validate the network. Therefore, the trained network might not be applicable to other datasets. Another limitation is that parameters for Elastix registration were possibly not optimal for each individual registration. As the craniosynostosis cases in the dataset are very diverse in appearance,

it is difficult to find one set of optimal parameters for all subjects. Therefore, parameters for Elastix registration were chosen such that MRI scans belonging to the four different categories described in section 3.4 (Qualitative Experiments), were visually registered well. Five MRI scans were evaluated per category. A last limitation of this study is that no re-sampling of the train, validate and test data, and no re-training of the network was performed to assess the variance in registration. Therefore, the standard errors and confidence intervals of the registration accuracy are unknown and the network could possibly be over-trained on the dataset.

### 5.3 Further Research

Overall, the outline of the head shape and ventricle shape of children with craniosynostosis were registered well, especially when using VoxelMorph. However, for use in clinical studies, better alignment of the cortical brain regions is required. In further research, the VoxelMorph neural network could possibly be improved by adjusting it to register the cortical surface, for example by using a spherical representation [31]. Additionally, re-sampling and re-training of the network should be carried out to assess registration variance, as well as validation of the network on an external dataset.

## 6 Conclusion

For registration of atlas MRI scans to MRI scans of children with craniosynostosis the best results were obtained using a learning-based method, as it was able to learn spatial prior information in the training process. In addition, when registering infant craniosynostosis scans, the use of infant atlases based on T2-weighted scans is advised. Regarding cortical registration, both approaches performed sub-optimal, and consequently further research is needed towards optimizing correct cortical registration. Such improved cortical registration is essential for the use of this method for the analysis of advanced MRI data in clinical studies of children with craniosynostosis.

## References

1. Johnson, D., Wilkie, A.O.M.: Craniosynostosis. *Eur J Hum Genet* **19** (2011)
2. Cornelissen, M., den Ottelander, B., Rizopoulos, D., et al.: Increase of prevalence of craniosynostosis. *J Cranio Maxill Surg* **44** (2016)
3. Mathijssen, I.M.: Guideline for care of patients with the diagnoses of craniosynostosis. *J Craniofac Surg* **26** (2015)
4. Mandela, R., Bellew, M., Chumas, P., Nash, H.: Impact of surgery timing for craniosynostosis on neurodevelopmental outcomes: a systematic review. *J Neurosurg-Pediatr* **23** (2019)
5. Hayward, R., Britto, J., Dunaway, D., Jeelani, O.: Connecting raised intracranial pressure and cognitive delay in craniosynostosis: many assumptions, little evidence. *J Neurosurg-Pediatr* **18** (2016)

6. Dickie, D.A., Shenkin, S.D., Anblagan, D., et al.: Whole brain magnetic resonance image atlases: A systematic review of existing atlases and caveats for use in population imaging. *Front Neuroinform* (2017)
7. Makropoulos, A., Aljabar, P., Wright, R., et al.: Regional growth and atlasing of the developing human brain. *NeuroImage* **125** (2016)
8. Knickmeyer, R.C., Gouttard, S., Kang, C., et al.: A structural mri study of human brain development from birth to 2 years. *J Neurosci* **28** (2008)
9. Dubois, J., Dehaene-Lambertz, G., Kulikova, S., et al.: The early development of brain white matter: A review of imaging studies in fetuses, newborns and infants. *Neuroscience* **276** (2014)
10. Haskins, G., Kruger, U., Yan, P.: Deep learning in medical image registration: a survey. *Mach Vision Appl* **31** (2020)
11. Balakrishnan, G., Zhao, A., Sabuncu, M.R., et al.: Voxelmorph: A learning framework for deformable medical image registration. *IEEE T Med Imaging* **38** (2019)
12. Wei, D., Ahmad, S., Huang, Y., et al.: An auto-context deformable registration network for infant brain mri (2020)
13. Ding, Y., Acosta, R., Enguix, V., et al.: Using deep convolutional neural networks for neonatal brain image segmentation. *Front Neurosci* **14** (2020)
14. Smith, N.: Introduction to medical imaging : physics, engineering and clinical applications. Cambridge University Press, Cambridge, UK New York (2011)
15. Barkovich, A.J.: Magnetic resonance techniques in the assessment of myelin and myelination. *Journal of Inherited Metabolic Disease* **28**(3), 311–343 (2005)
16. Holland, D., Chang, L., Ernst, T.M., Curran, M., Buchthal, S.D., Alicata, D., Skranes, J., Johansen, H., Hernandez, A., Yamakawa, R., Kuperman, J.M., Dale, A.M.: Structural growth trajectories and rates of change in the first 3 months of infant brain development. *JAMA Neurology* **71**(10), 1266 (2014)
17. Wang, L., Nie, D., Li, G., Puybareau, E., Dolz, J., Zhang, Q., Wang, F., Xia, J., Wu, Z., Chen, J.W., Thung, K.H., Bui, T.D., Shin, J., Zeng, G., Zheng, G., Fonov, V.S., Doyle, A., Xu, Y., Moeskops, P., Pluim, J.P.W., Desrosiers, C., Aved, I.B., Sanroma, G., Benkarim, O.M., Casamitjana, A., Vilaplana, V., Lin, W., Li, G., Shen, D.: Benchmark on automatic six-month-old infant brain segmentation algorithms: The iSeg-2017 challenge. *IEEE T Med Imaging* **38**(9), 2219–2230 (2019)
18. Oishi, K., Chang, L., Huang, H.: Baby brain atlases. *NeuroImage* **185**, 865–880 (2019)
19. Alexander, B., Murray, A.L., Loh, W.Y., et al.: A new neonatal cortical and sub-cortical brain atlas: the melbourne children's regional infant brain (m-CRIB) atlas. *NeuroImage* **147** (2017)
20. Gousias, I.S., Edwards, A.D., Rutherford, M.A., Counsell, S.J., Hajnal, J.V., Rueckert, D., Hammers, A.: Magnetic resonance imaging of the newborn brain: Manual segmentation of labelled atlases in term-born and preterm infants. *NeuroImage* **62**(3), 1499–1509 (2012)
21. Oliveira, F.P., Tavares, J.M.R.: Medical image registration: a review. *Computer Methods in Biomechanics and Biomedical Engineering* **17**(2), 73–93 (2012)
22. Sotiras, A., Davatzikos, C., Paragios, N.: Deformable medical image registration: A survey. *IEEE Transactions on Medical Imaging* **32**(7), 1153–1190 (2013)
23. Klein, S., Staring, M., Murphy, K., et al.: elastix: A toolbox for intensity-based medical image registration. *IEEE T Med Imaging* **29** (2010)
24. Fischl, B.: FreeSurfer. *NeuroImage* **62** (2012)
25. Ikram, M.A., Brusselle, G.G.O., Murad, S.D., et al.: The rotterdam study: 2018 update on objectives, design and main results. *Eur J Epidemiol* **32** (2017)

26. Wong, S.C., Gatt, A., Stamatescu, V., McDonnell, M.D.: Understanding data augmentation for classification: when to warp? (2016)
27. Tustison, N.J., Avants, B.B., Cook, P.A., et al.: N4itk: Improved n3 bias correction. *IEEE T Med Imaging* **29** (2010)
28. Abraham, A., Pedregosa, F., Eickenberg, M., Gervais, P., Mueller, A., Kossaifi, J., Gramfort, A., Thirion, B., Varoquaux, G.: Machine learning for neuroimaging with scikit-learn. *Frontiers in Neuroinformatics* **8** (2014)
29. Smith, S.M.: Fast robust automated brain extraction. *Human Brain Mapping* **17** (2002)
30. Klein, A., Andersson, J., Ardekani, B.A., Ashburner, J., Avants, B., Chiang, M.C., Christensen, G.E., Collins, D.L., Gee, J., Hellier, P., Song, J.H., Jenkinson, M., Lepage, C., Rueckert, D., Thompson, P., Vercauteren, T., Woods, R.P., Mann, J.J., Parsey, R.V.: Evaluation of 14 nonlinear deformation algorithms applied to human brain MRI registration **46**(3), 786–802 (2009)
31. Cheng, J., Dalca, A.V., Fischl, B., Zöllei, L.: Cortical surface registration using unsupervised learning. *NeuroImage* **221** (2020)

## 7 Appendices

### 7.1 Appendix A — Synthetic Data

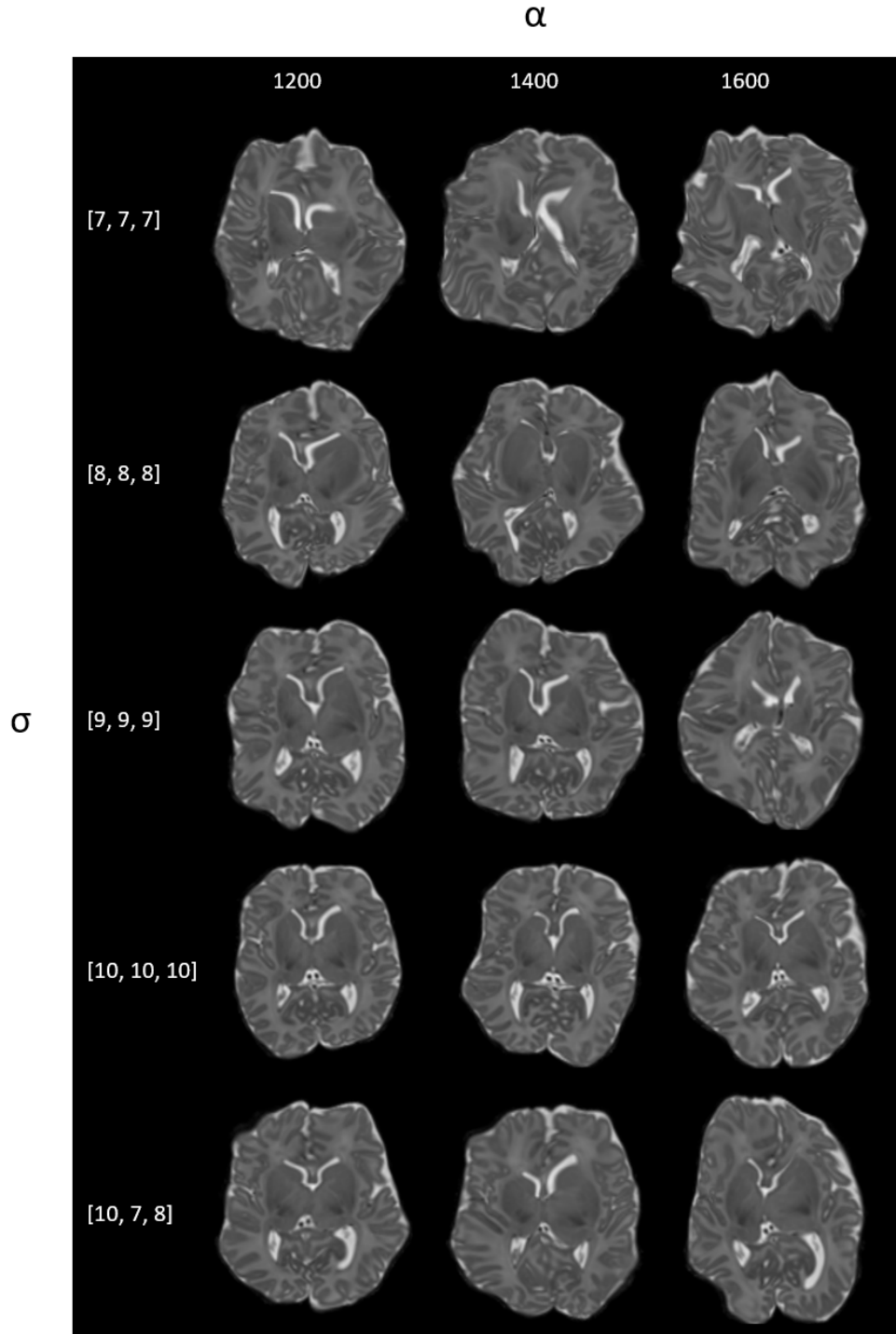


**Fig. 14.** T2w images of synthetic data created from the infant atlas, with varying values of  $\alpha$  and  $\sigma$ . When creating the synthetic data, three random values are used for  $\sigma$ .

## 7.2 Appendix B — Brain Areas

Table 2: Division of both infant and adult atlas brain labels into different brain areas.

Brain Area	Brain Label Number	Brain Label
White Matter	2	Left Cerebral White Matter
	41	Right Cerebral White Matter
Ventricles	4	Left Lateral Ventricle
	14	3rd Ventricle
	15	4th Ventricle
	43	Right Lateral Ventricle
Cerebellum	7	Left Cerebellum White Matter
	8	Left Cerebellum Cortex
	46	Right Cerebellum White Matter
	47	Right Cerebellum Cortex
	75	Cerebellar Vermis Superior Posterior
	76	Cerebellar Vermis Anterior
	91	Left Cerebellar Hemisphere
Brain Stem	93	Right Cerebellar Hemisphere
	16	Brain Stem
WM Structures	170	Brain Stem
	9	Left Thalamus
	10	Left Thalamus
	11	Left Caudate
	12	Left Putamen
	13	Left Pallidum
	17	Left Hippocampus
	18	Left Amygdala
	26	Left Accubens Area
	48	Right Thalamus
	49	Right Thalamus
	50	Right Caudate
	51	Right Putamen
	52	Right Pallidum
	53	Right Hippocampus
	54	Right Amygdala
	58	Right Accubens Area
	192	Corpus Callosum
	251	Corpus Callosum Posterior
	252	Corpus Callosum Mid Posterior
253	Corpus Callosum Central	
254	Corpus Callosum Mid Anterior	
255	Corpus Callosum Anterior	

Table 2: (continued)

Brain Area	Brain Label Number	Brain Label
Temporal Cortex	1006	Left Entorhinal Cortex
	1007	Left Fusiform Cortex
	1009	Left Inferior Temporal Cortex
	1015	Left Middle Temporal Cortex
	1016	Left Parahippocampal Cortex
	1030	Left Superior Temporal Cortex
	1033	Left Temporal Pole
	1034	Left Transverse Temporal Cortex
	2006	Right Entorhinal Cortex
	2007	Right Fusiform Cortex
	2009	Right Inferior Temporal Cortex
	2015	Right Middle Temporal Cortex
	2016	Right Parahippocampal Cortex
	2030	Right Superior Temporal Cortex
	2033	Right Transverse Temporal Cortex
	2034	Right Temporal Pole
Frontal Cortex	1003	Left Caudal Middle Frontal Cortex
	1012	Left Lateral Orbito Frontal Cortex
	1014	Left Medial Orbito Frontal Cortex
	1017	Left Paracentral Cortex
	1018	Left Pars Opercularis Cortex
	1019	Left Pars Orbitalis Cortex
	1020	Left Pars Triangularis Cortex
	1024	Left Precentral Cortex
	1027	Left Rostral Middle Frontal Cortex
	1028	Left Superior Frontal Cortex
	1032	Left Frontal Pole
	2003	Right Caudal Middle Frontal Cortex
	2012	Right Lateral Orbito Frontal Cortex
	2014	Right Medial Orbito Frontal Cortex
	2017	Right Paracentral Cortex
	2018	Right Pars Opercularis Cortex
	2019	Right Pars Orbitalis Cortex
	2020	Right Pars Triangularis Cortex
	2024	Right Precentral Cortex
	2027	Right Rostral Middle Frontal Cortex
2028	Right Superior Frontal Cortex	
2032	Right Frontal Pole	
Parietal Cortex	1008	Left Inferior Parietal Cortex
	1022	Left Postcentral Cortex
	1025	Left Precuneus Cortex
	1029	Left Superior Parietal Cortex
	1031	Left Supramarginal Cortex

Table 2: (continued)

Brain Area	Brain Label Number	Brain Label
	2008	Right Inferior Parietal Cortex
	2022	Right Postcentral Cortex
	2025	Right Precuneus Cortex
	2029	Right Superior Parietal Cortex
	2031	Right Supramarginal Cortex
	1005	Left Cuneus Cortex
	1011	Left Lateral Occipital Cortex
	1013	Left Lingual Cortex
Occipital Cortex	1021	Left Pericalcarine Cortex
	2005	Right Cuneus Cortex
	2011	Right Lateral Occipital Cortex
	2013	Right Lingual Cortex
	2026	Right Pericalcarine Cortex
	1002	Left Caudal Anterior Cingulate Cortex
	1010	Left Isthmus Cingulate Cortex
	1023	Left Posterior Cingulate Cortex
Cingulate Cortex	1026	Left Rostral Anterior Cingulate Cortex
	2002	Right Caudal Anterior Cingulate Cortex
	2010	Right Isthmus Cingulate Cortex
	2023	Right Posterior Cingulate Cortex
	2026	Right Rostral Anterior Cingulate Cortex

### 7.3 Appendix C — VoxelMorph Optimization Synthetic Data

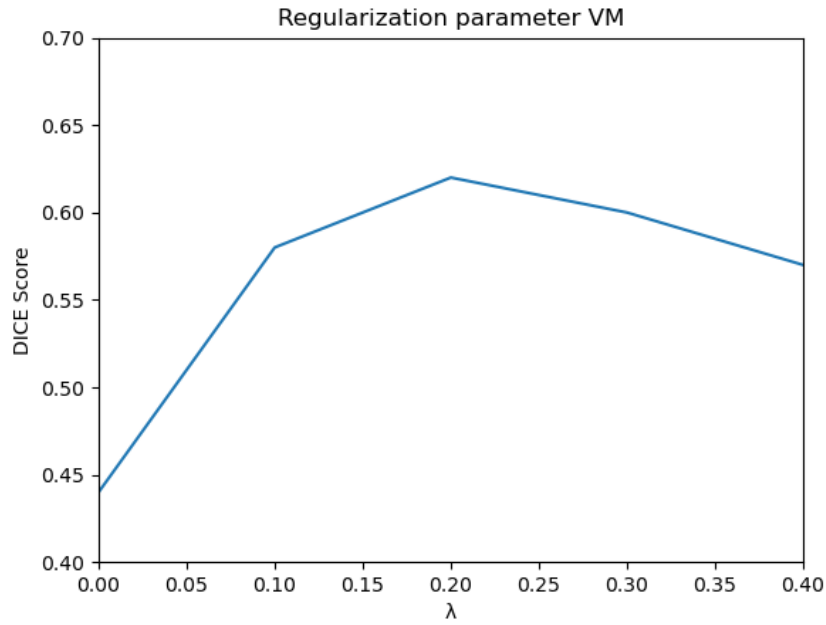


**Fig. 15.** DICE scores of synthetic validation data, registered using the network trained with T2w scans and the infant atlases, with varying parameter  $\lambda$ .

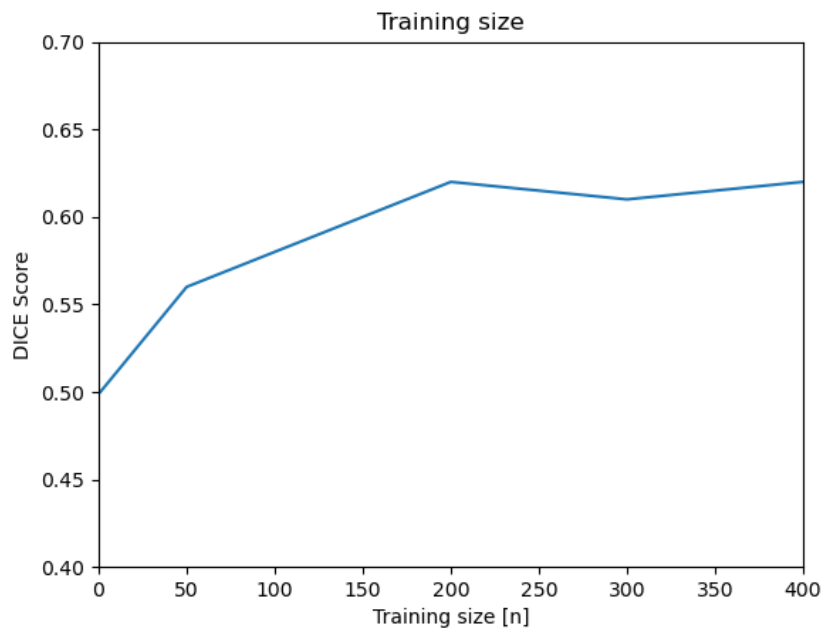


**Fig. 16.** DICE scores of synthetic validation data, registered using the network trained with T2w scans and the infant atlases, with varying training sizes.

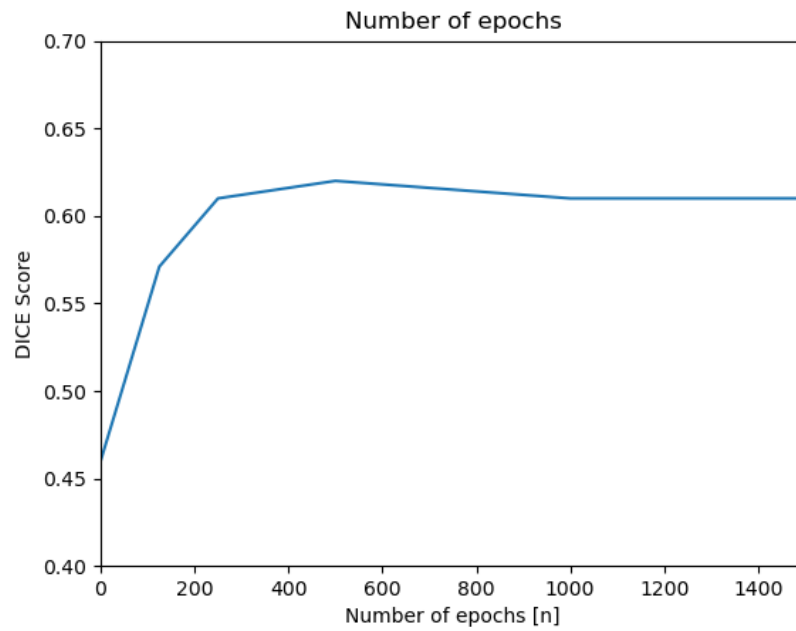


**Fig. 17.** DICE scores of synthetic validation data, registered using the network trained with T2w scans and the infant atlases, with a varying number of epochs.

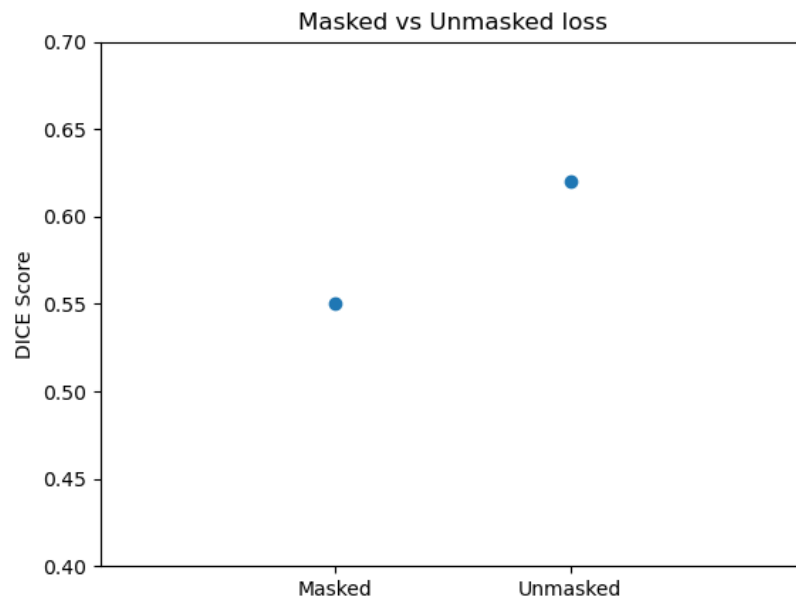


**Fig. 18.** DICE scores of synthetic validation data, registered using the network trained with T2w scans and the infant atlases, with a masked loss and unmasked loss.

#### 7.4 Appendix D — VoxelMorph Optimization Craniosynostosis Data

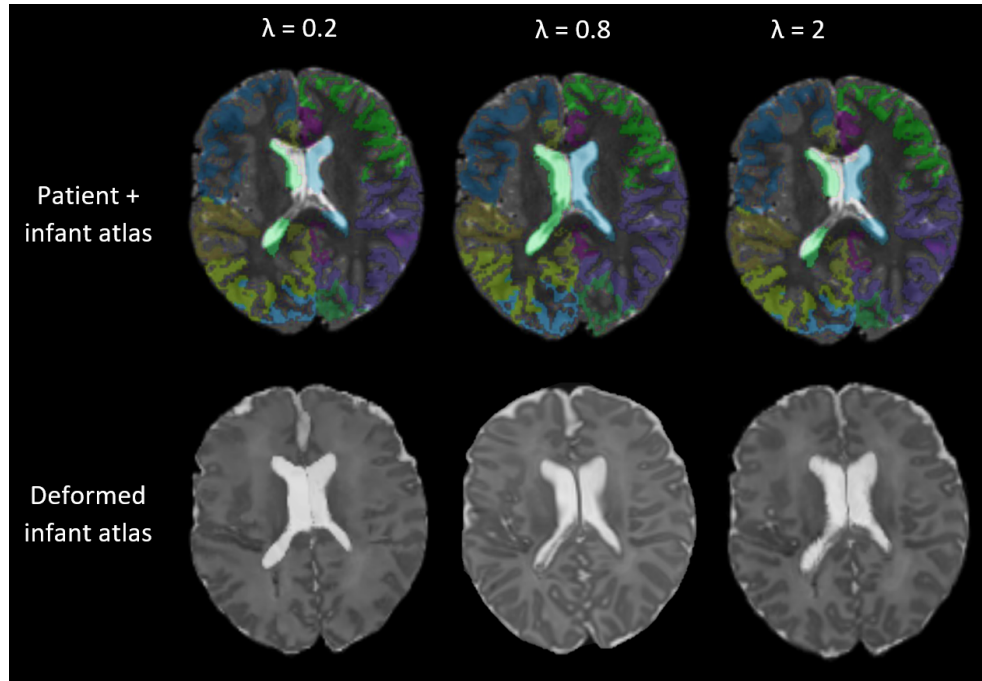


**Fig. 19.** T2w images of an infant atlas registered to a child with craniosynostosis using VoxelMorph. Both the deformed atlas scans and patient images with an overlay of the deformed brain regions are shown separately for registration using a  $\lambda$  of 0.2, 0.8 and 2. The brain pattern of this child is relatively old and normal looking.



## 7.5 Appendix E — Elastix Registration Synthetic Data

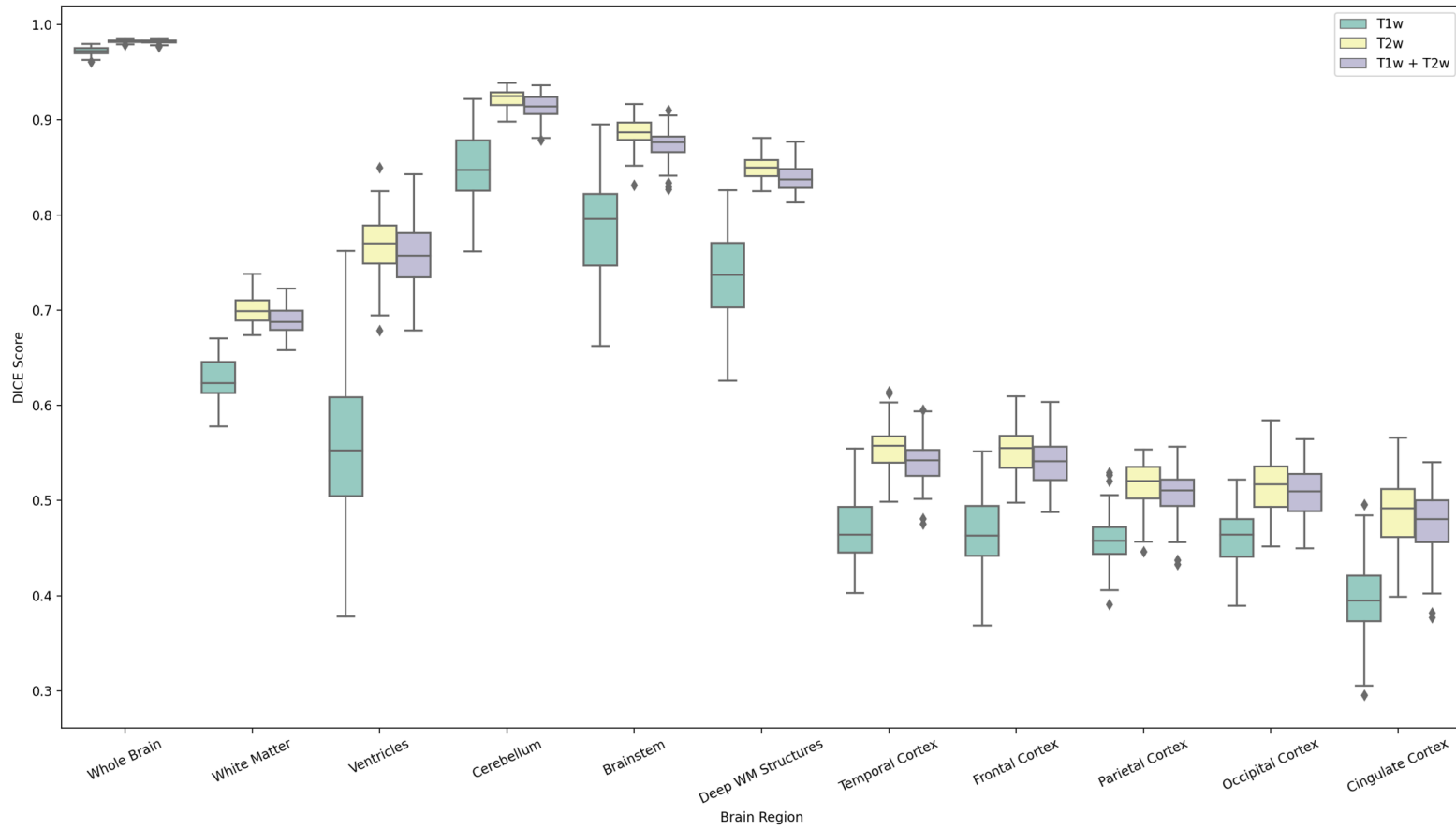


**Fig. 20.** Boxplots of DICE scores for various anatomical structures, resulting from Elastix registration performed on non-deformed infant atlases. Scores are shown separately for registration using T1w images, T2w images and both T1w and T2w images. DICE scores of left and right brain structures are averaged.

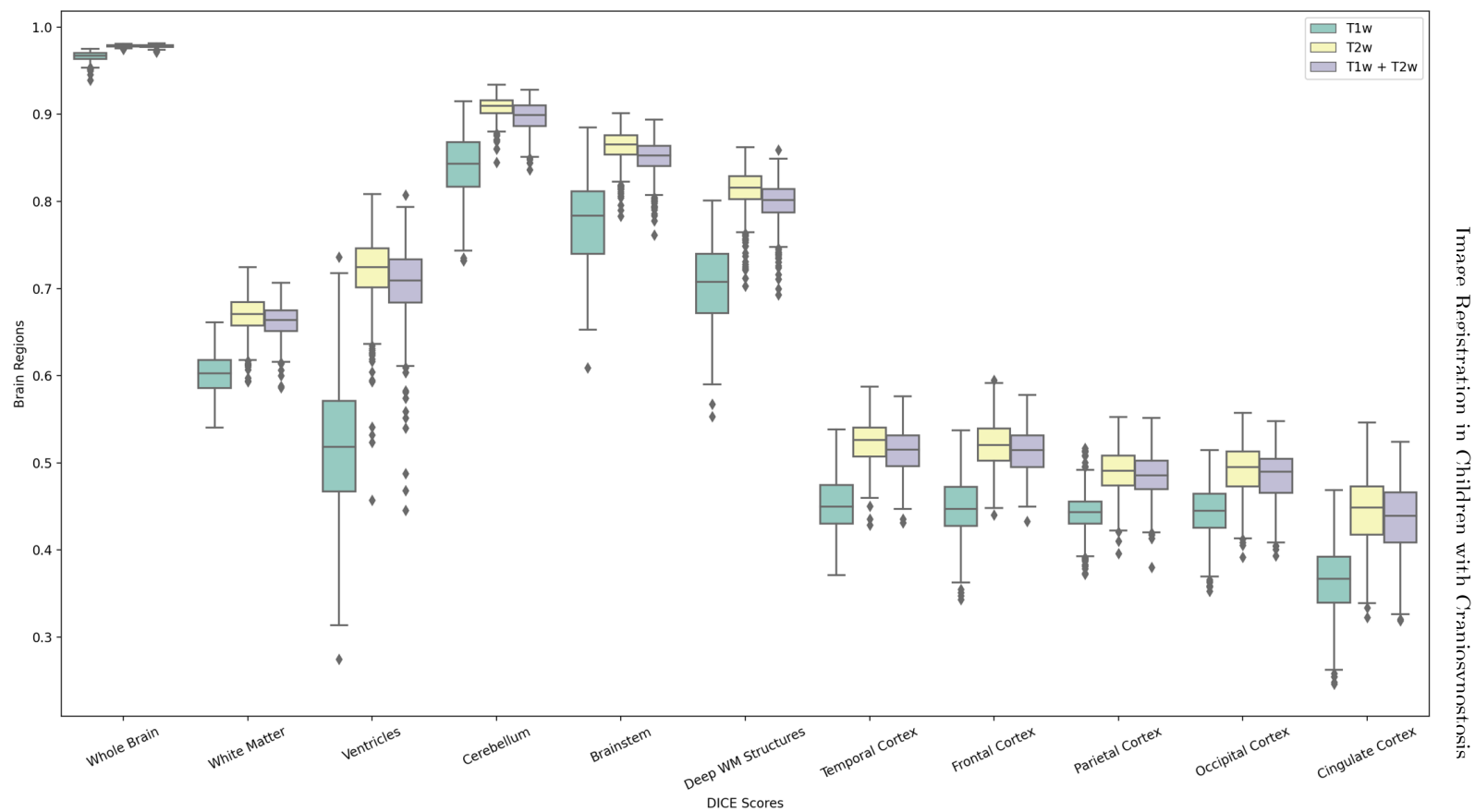


**Fig. 21.** Boxplots of DICE scores for various anatomical structures, resulting from Elastix registration performed on deformed infant atlases. Scores are shown separately for registration using T1w images, T2w images and both T1w and T2w images. DICE scores of left and right brain structures are averaged.

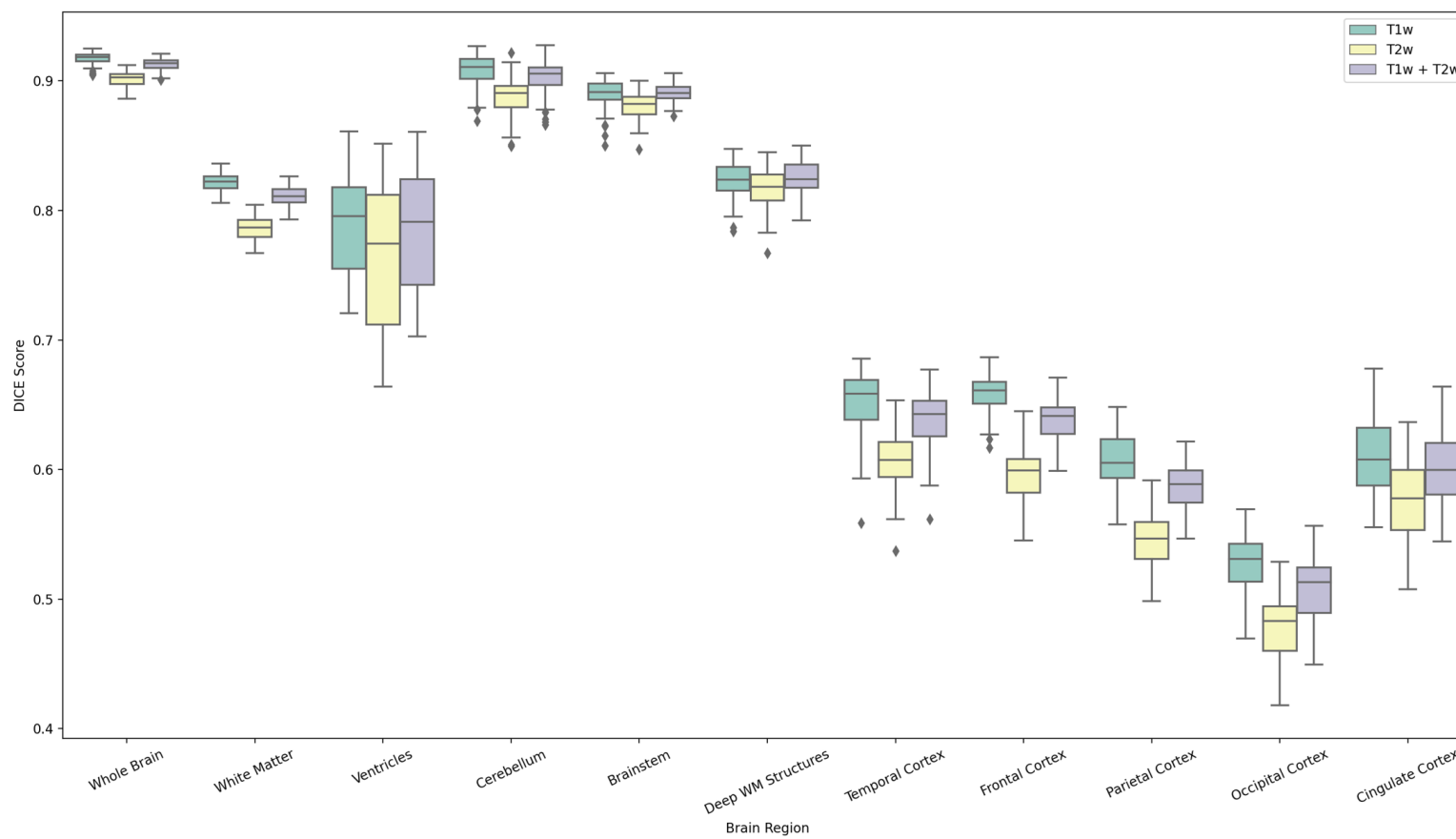


**Fig. 22.** Boxplots of DICE scores for various anatomical structures, resulting from Elastix registration performed on non-deformed adult atlases. Scores are shown separately for registration using T1w images, T2w images and both T1w and T2w images. DICE scores of left and right brain structures are averaged.

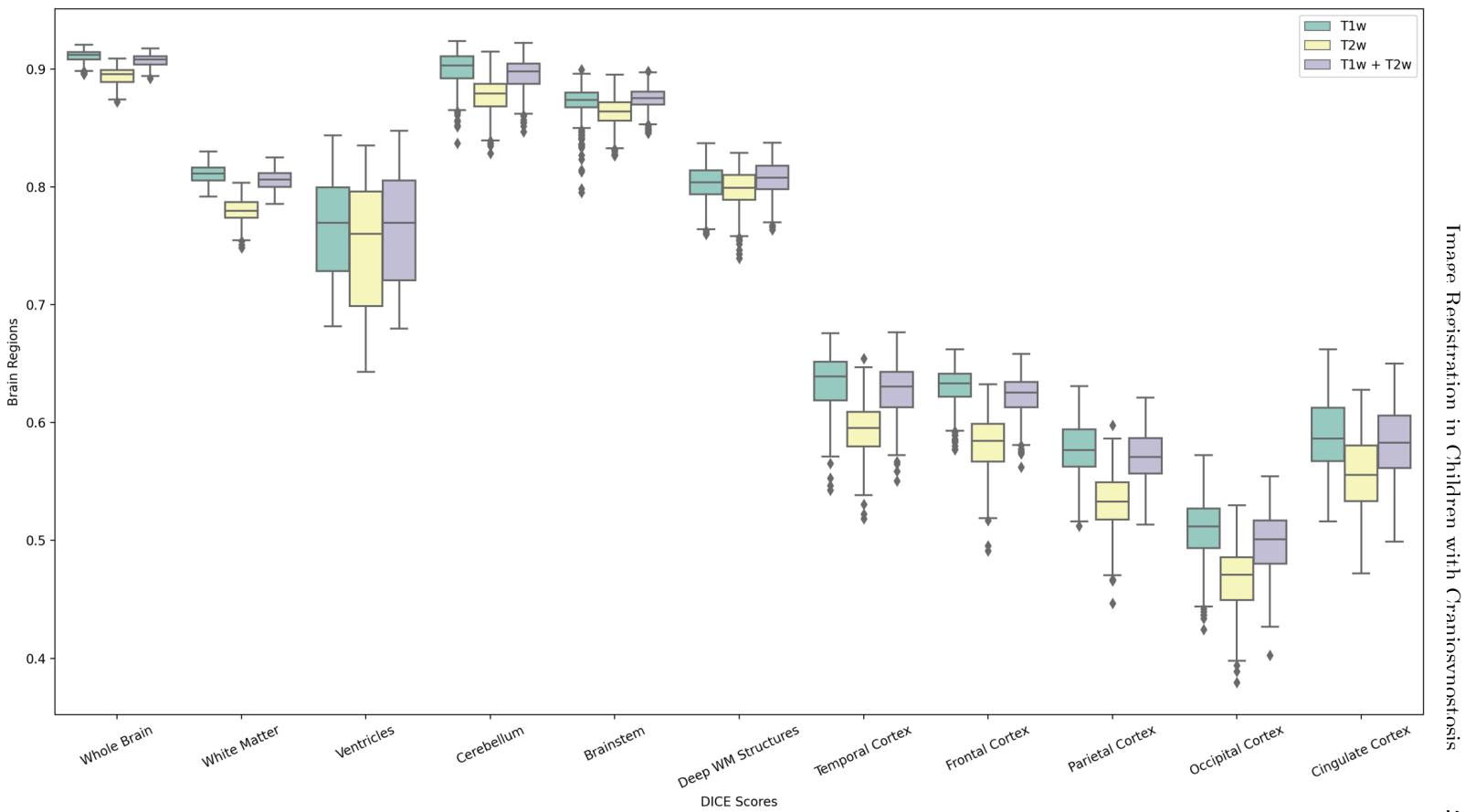


**Fig. 23.** Boxplots of DICE scores for various anatomical structures, resulting from Elastix registration performed on deformed adult atlases. Scores are shown separately for registration using T1w images, T2w images and both T1w and T2w images. DICE scores of left and right brain structures are averaged.



## 7.6 Appendix F — Elastix Registration Craniosynostosis Data

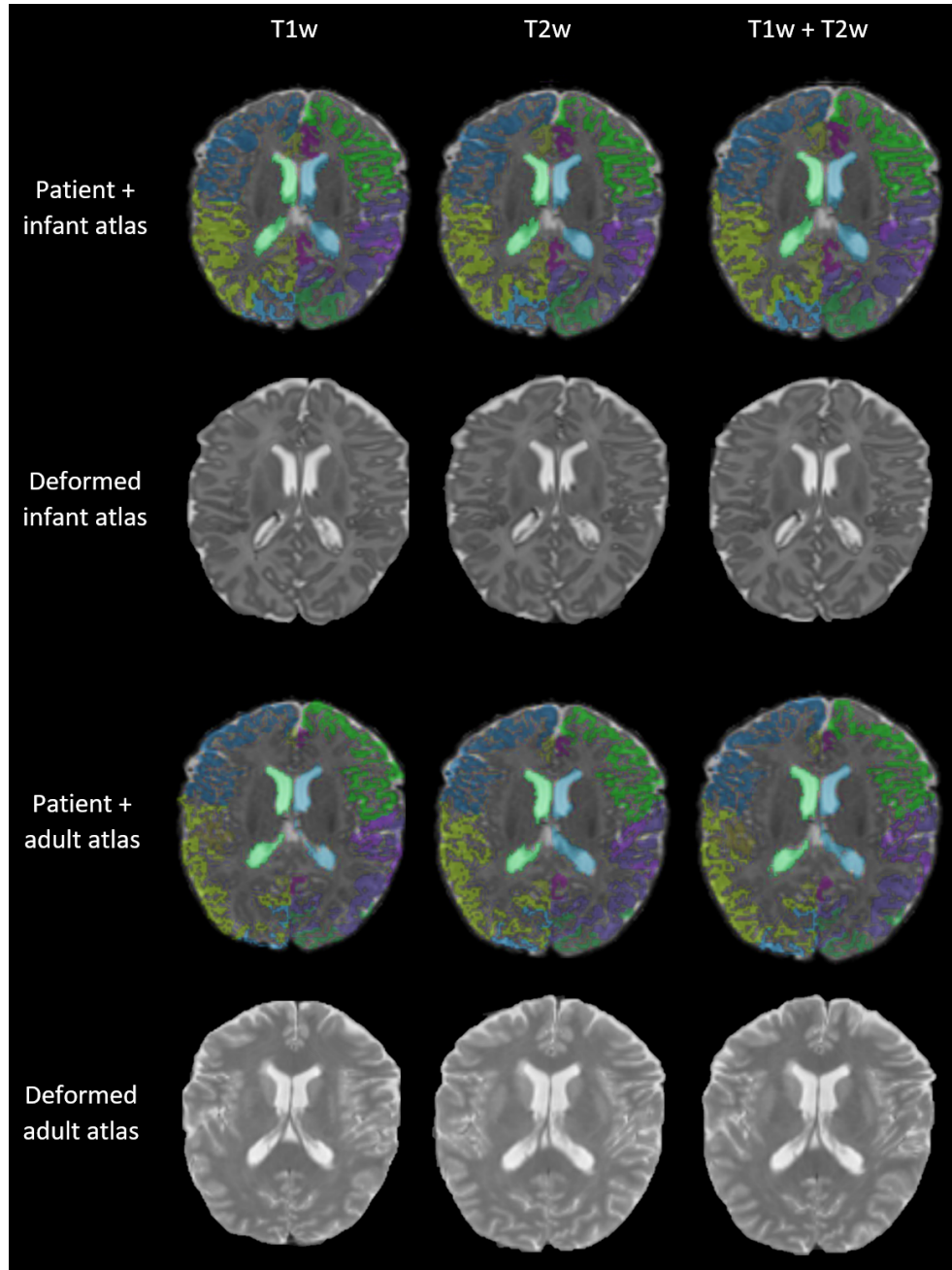


**Fig. 24.** T2w images of infant and adult atlases registered to a child with craniosynostosis using Elastix. Both the deformed atlas scans and patient images with an overlay of the deformed brain regions are shown separately for registration using T1w images, T2w images and both T1w and T2w images. The brain pattern of this child is relatively young and normal looking.

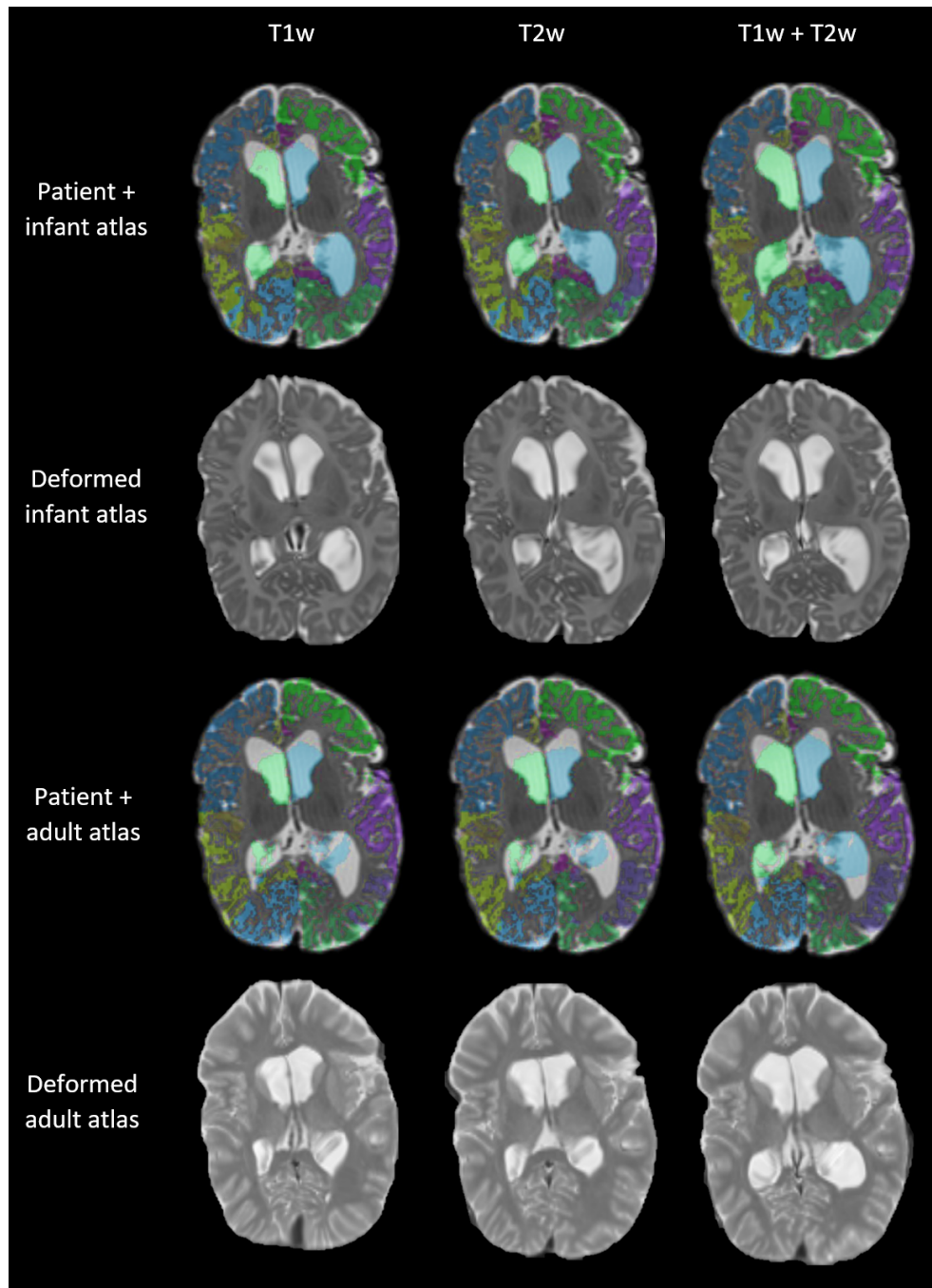


**Fig. 25.** T2w images of infant and adult atlases registered to a child with craniosynostosis using Elastix. Both the deformed atlas scans and patient images with an overlay of the deformed brain regions are shown separately for registration using T1w images, T2w images and both T1w and T2w images. The brain pattern of this child is relatively young and abnormal looking.

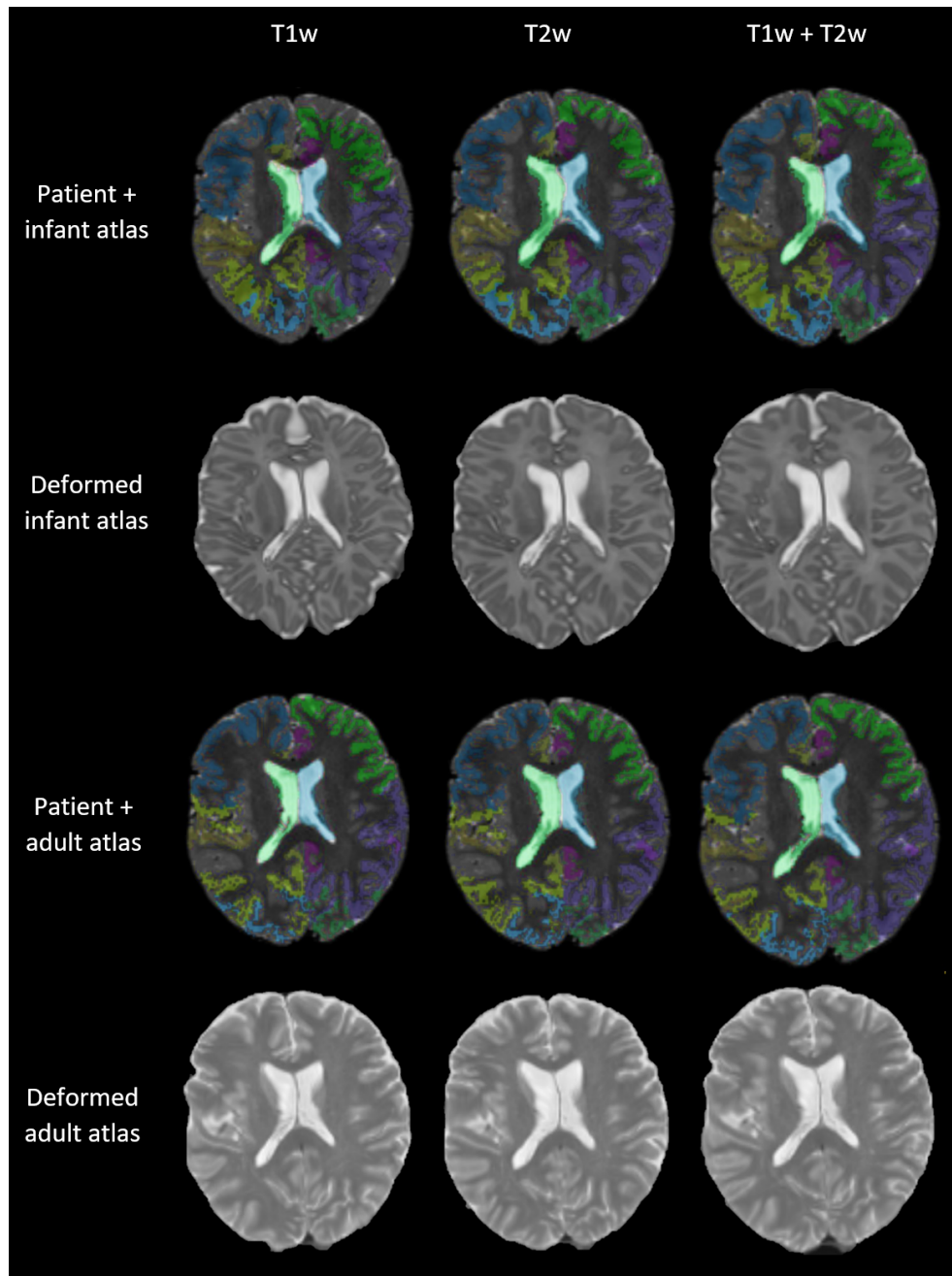


**Fig. 26.** T2w images of infant and adult atlases registered to a child with craniosynostosis using Elastix. Both the deformed atlas scans and patient images with an overlay of the deformed brain regions are shown separately for registration using T1w images, T2w images and both T1w and T2w images. The brain pattern of this child is relatively old and normal looking.

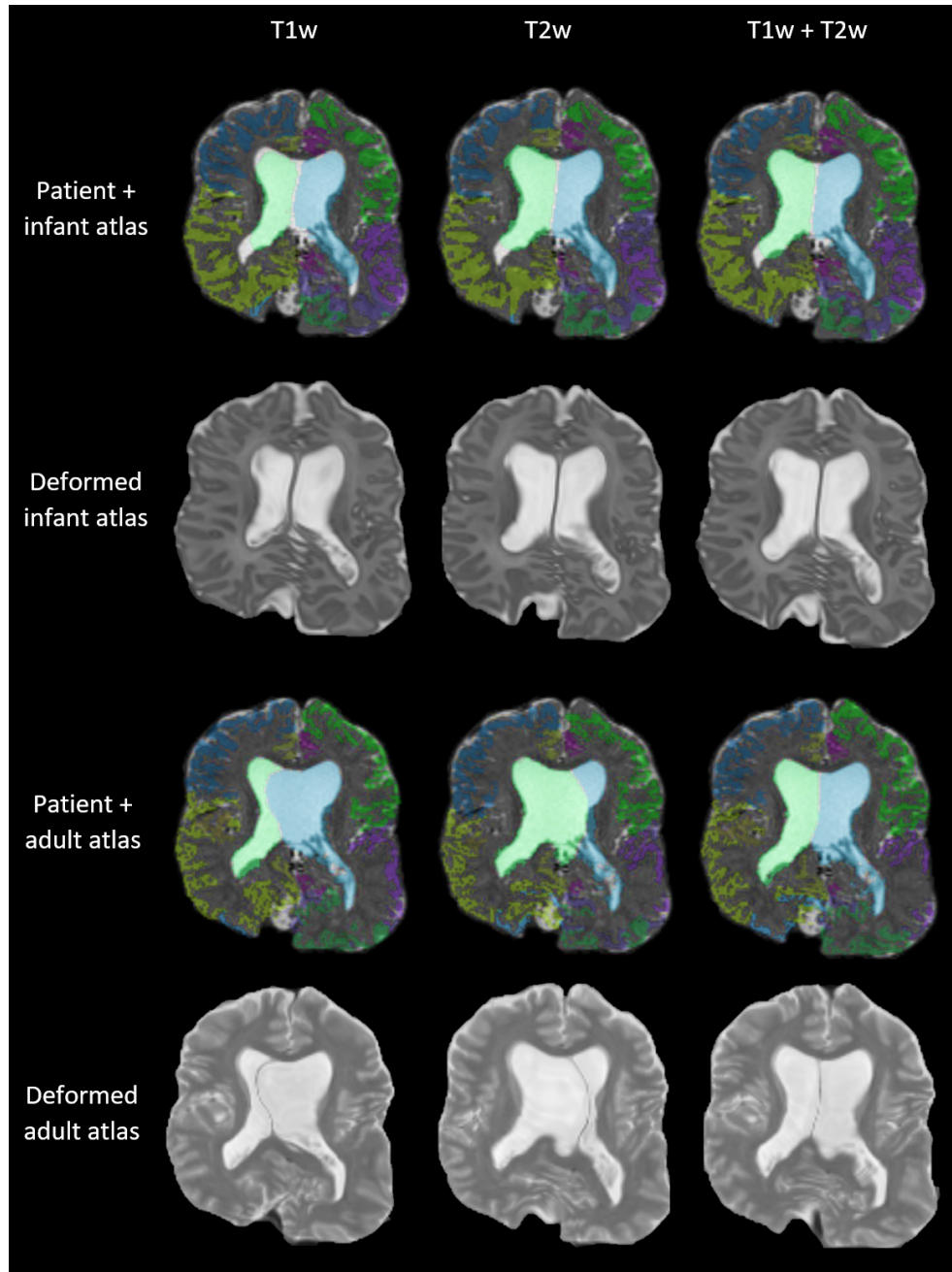


**Fig. 27.** T2w images of infant and adult atlases registered to a child with craniosynostosis using Elastix. Both the deformed atlas scans and patient images with an overlay of the deformed brain regions are shown separately for registration using T1w images, T2w images and both T1w and T2w images. The brain pattern of this child is relatively old and abnormal looking.



## 7.7 Appendix G — VoxelMorph Registration Synthetic Data

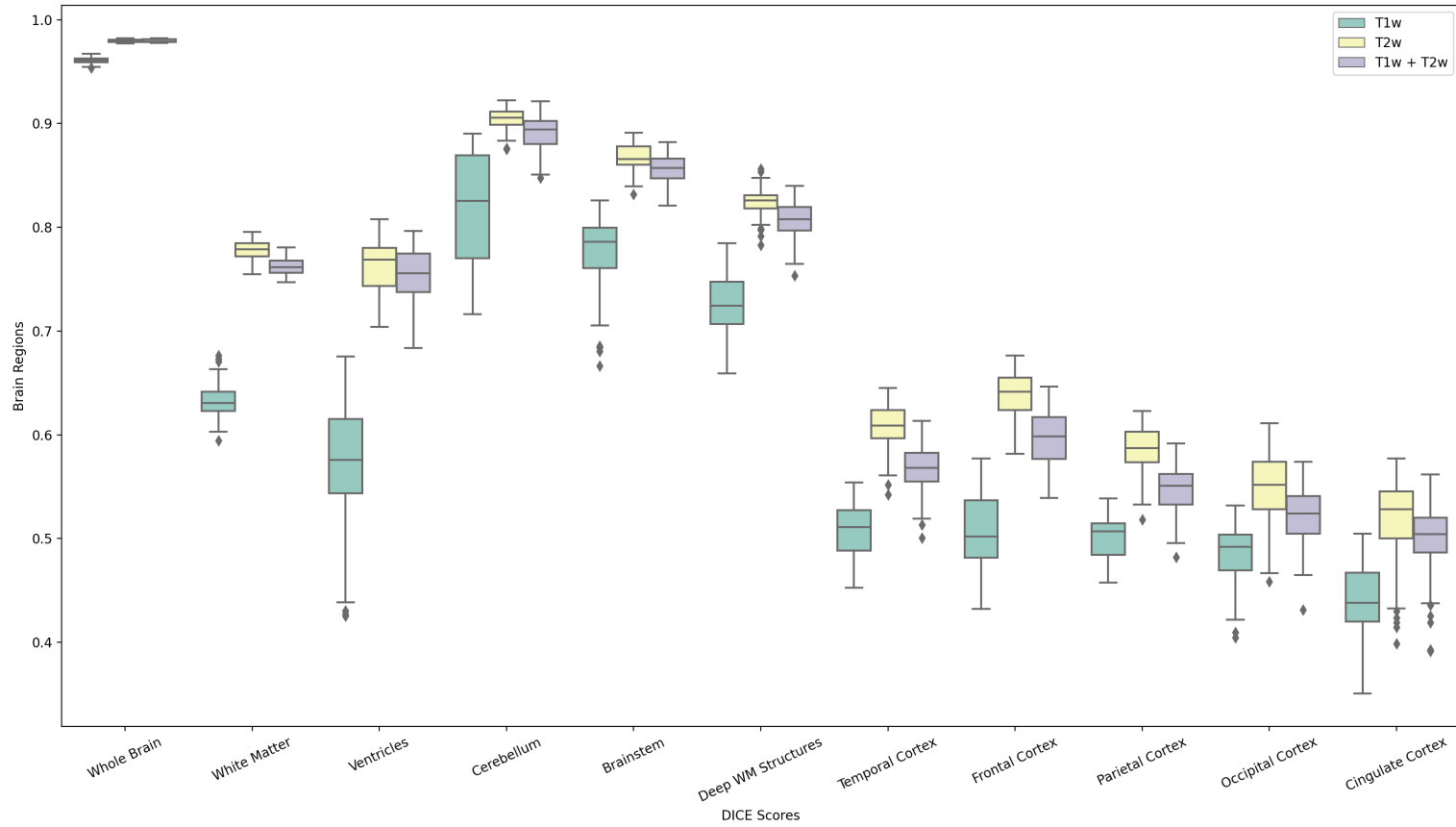


**Fig. 28.** Boxplots of DICE scores for various anatomical structures, resulting from VoxelMorph registration performed on non-deformed infant atlases. Scores are shown separately for registration using T1w images, T2w images and both T1w and T2w images. DICE scores of left and right brain structures are averaged.

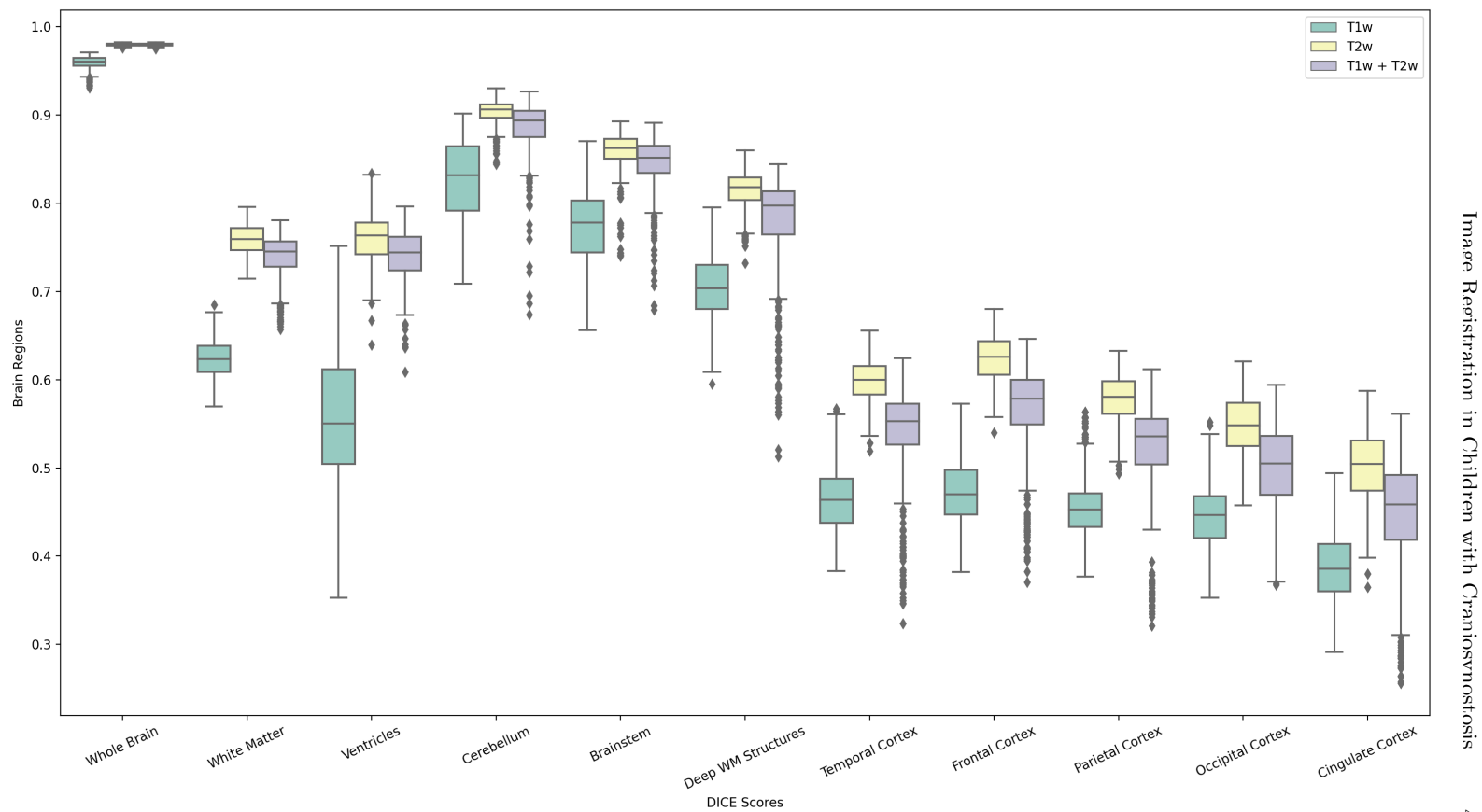


**Fig. 29.** Boxplots of DICE scores for various anatomical structures, resulting from VoxelMorph registration performed on deformed infant atlases. Scores are shown separately for registration using T1w images, T2w images and both T1w and T2w images. DICE scores of left and right brain structures are averaged.

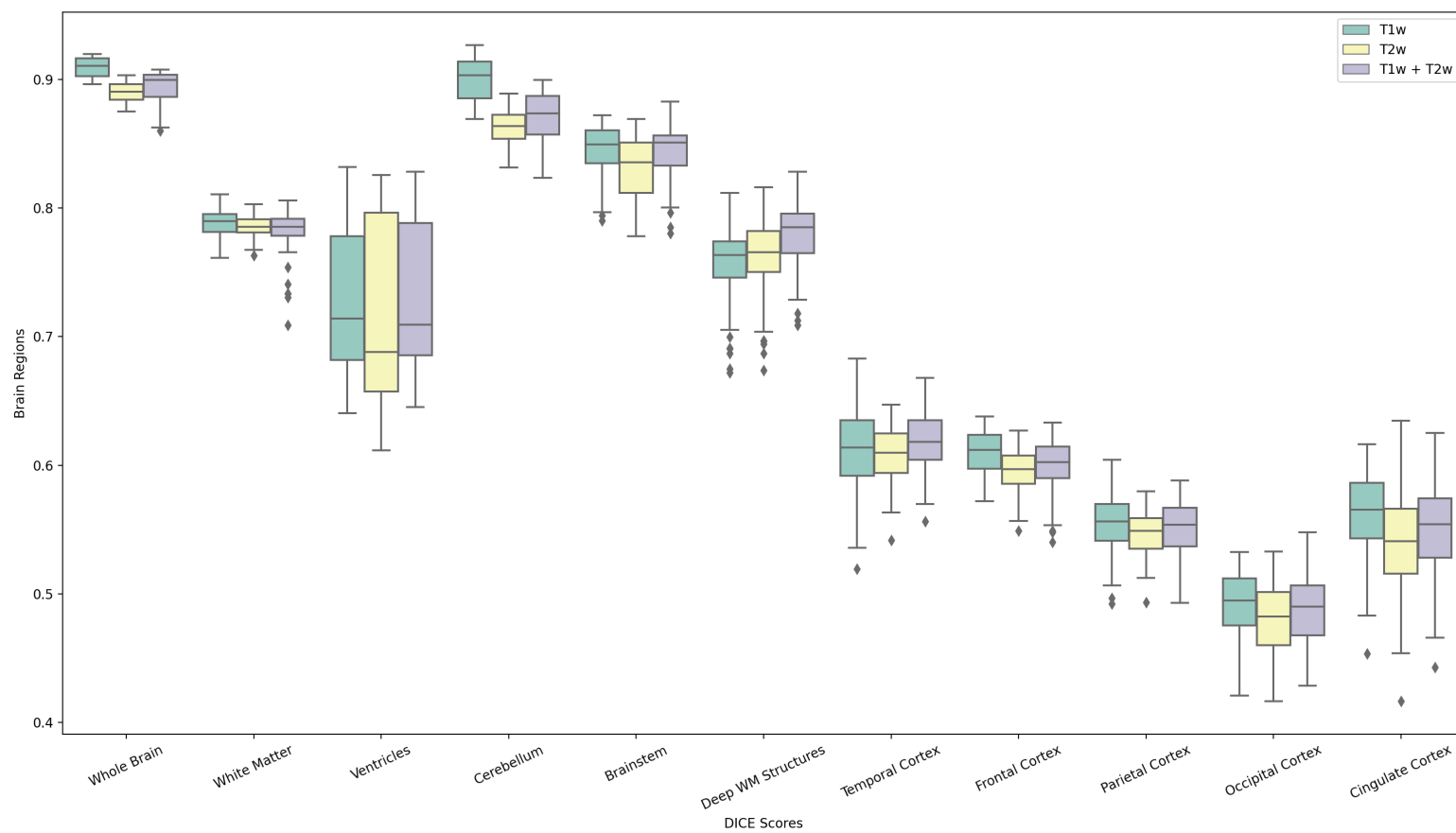


**Fig. 30.** Boxplots of DICE scores for various anatomical structures, resulting from VoxelMorph registration performed on non-deformed adult atlases. Scores are shown separately for registration using T1w images, T2w images and both T1w and T2w images. DICE scores of left and right brain structures are averaged.

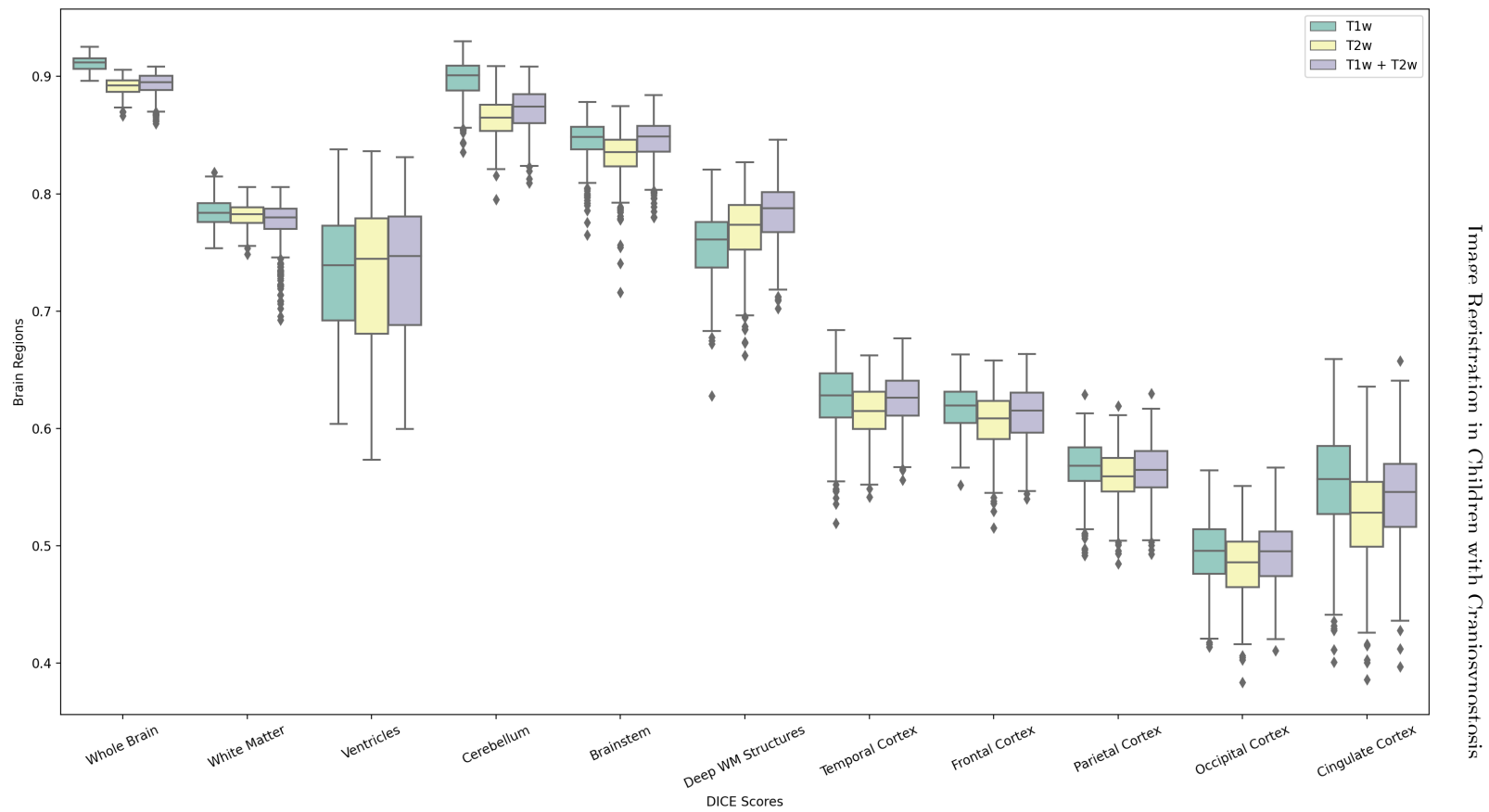


**Fig. 31.** Boxplots of DICE scores for various anatomical structures, resulting from VoxelMorph registration performed on deformed adult atlases. Scores are shown separately for registration using T1w images, T2w images and both T1w and T2w images. DICE scores of left and right brain structures are averaged.



## 7.8 Appendix H — VoxelMorph Registration Craniosynostosis Data

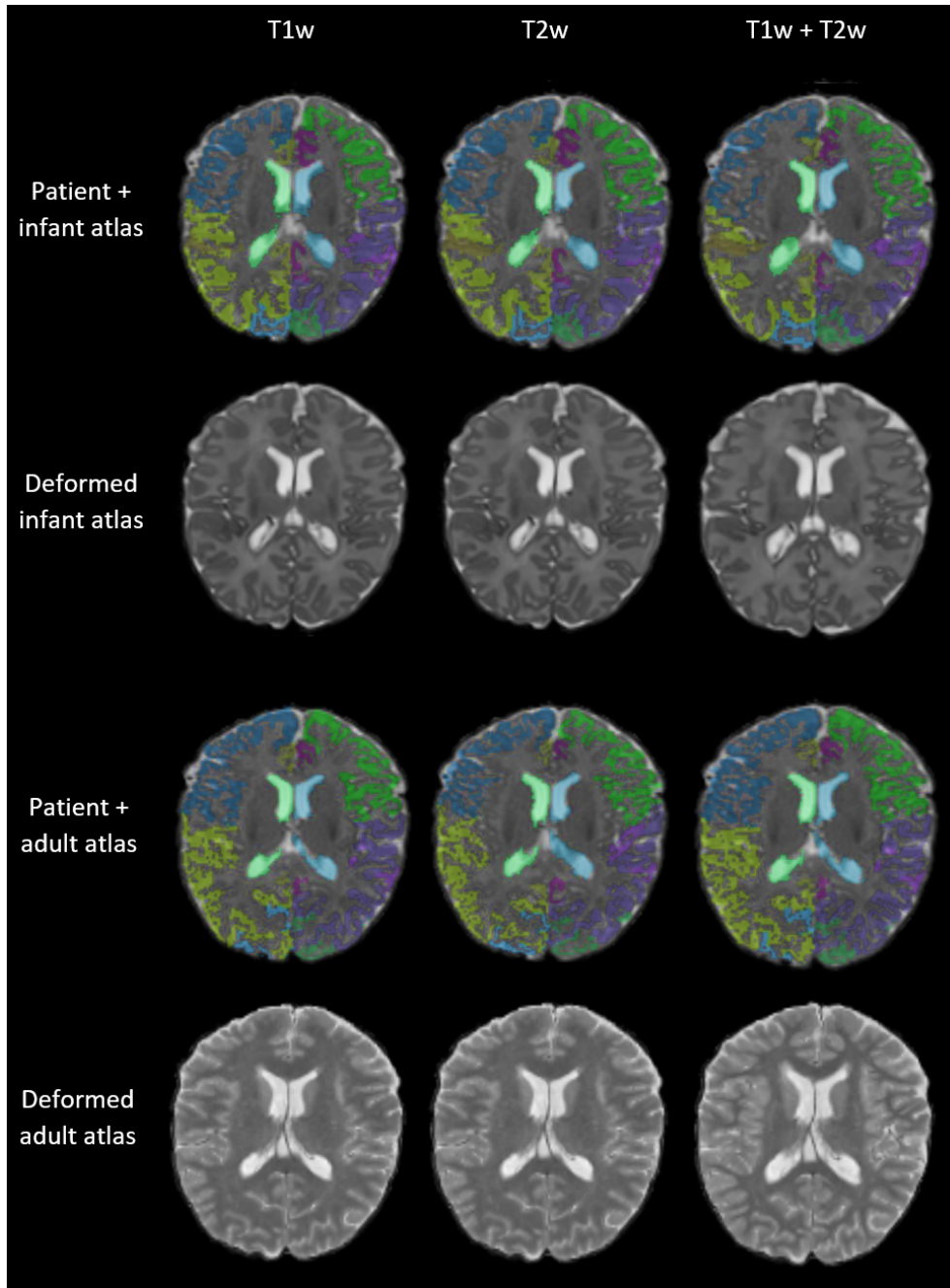


**Fig. 32.** T2w images of infant and adult atlases registered to a child with craniosynostosis using VoxelMorph. Both the deformed atlas scans and patient images with an overlay of the deformed brain regions are shown separately for registration using T1w images, T2w images and both T1w and T2w images. The brain pattern of this child is relatively young and normal looking.

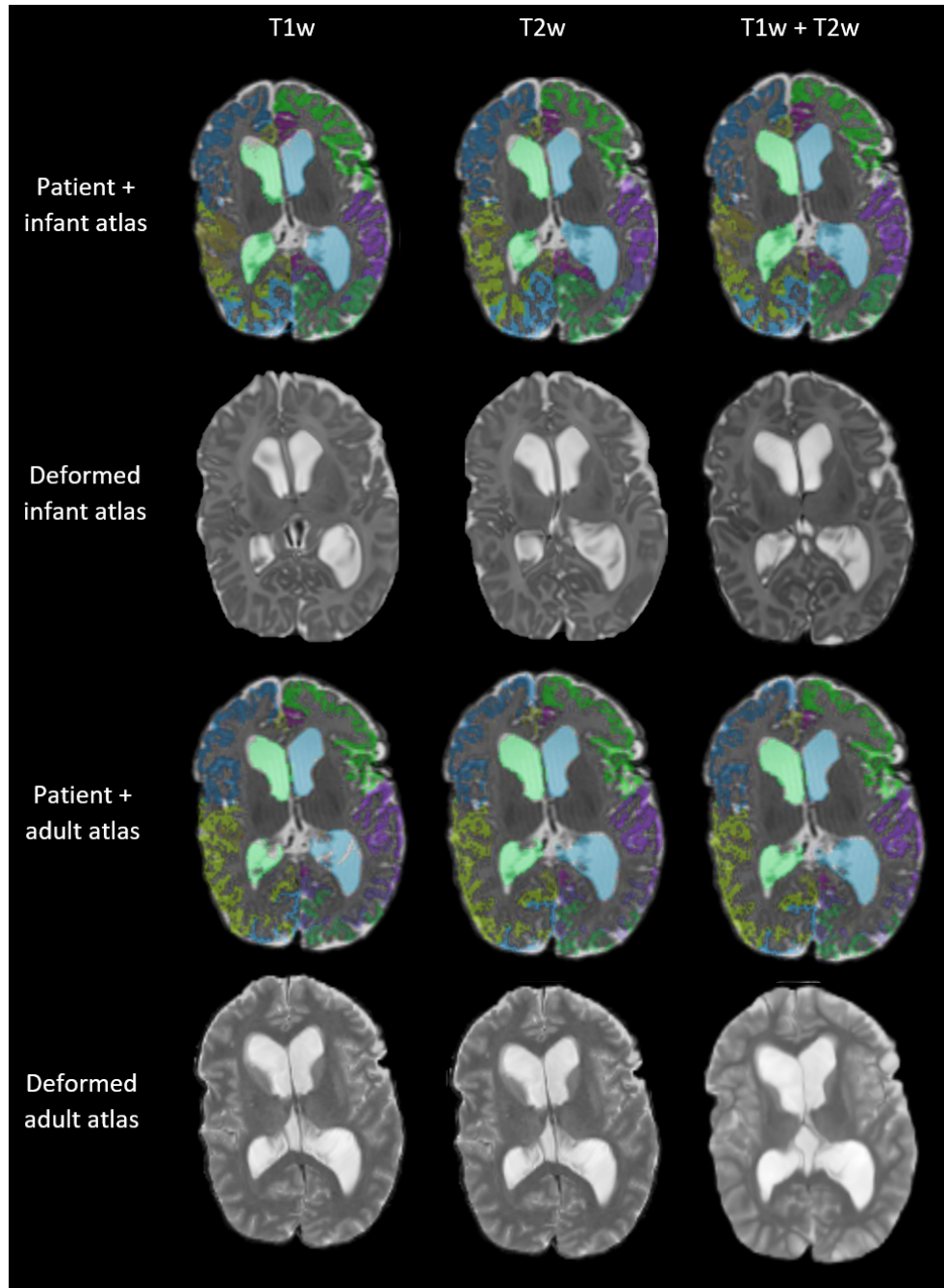


**Fig. 33.** T2w images of infant and adult atlases registered to a child with craniosynostosis using VoxelMorph. Both the deformed atlas scans and patient images with an overlay of the deformed brain regions are shown separately for registration using T1w images, T2w images and both T1w and T2w images. The brain pattern of this child is relatively young and abnormal looking.

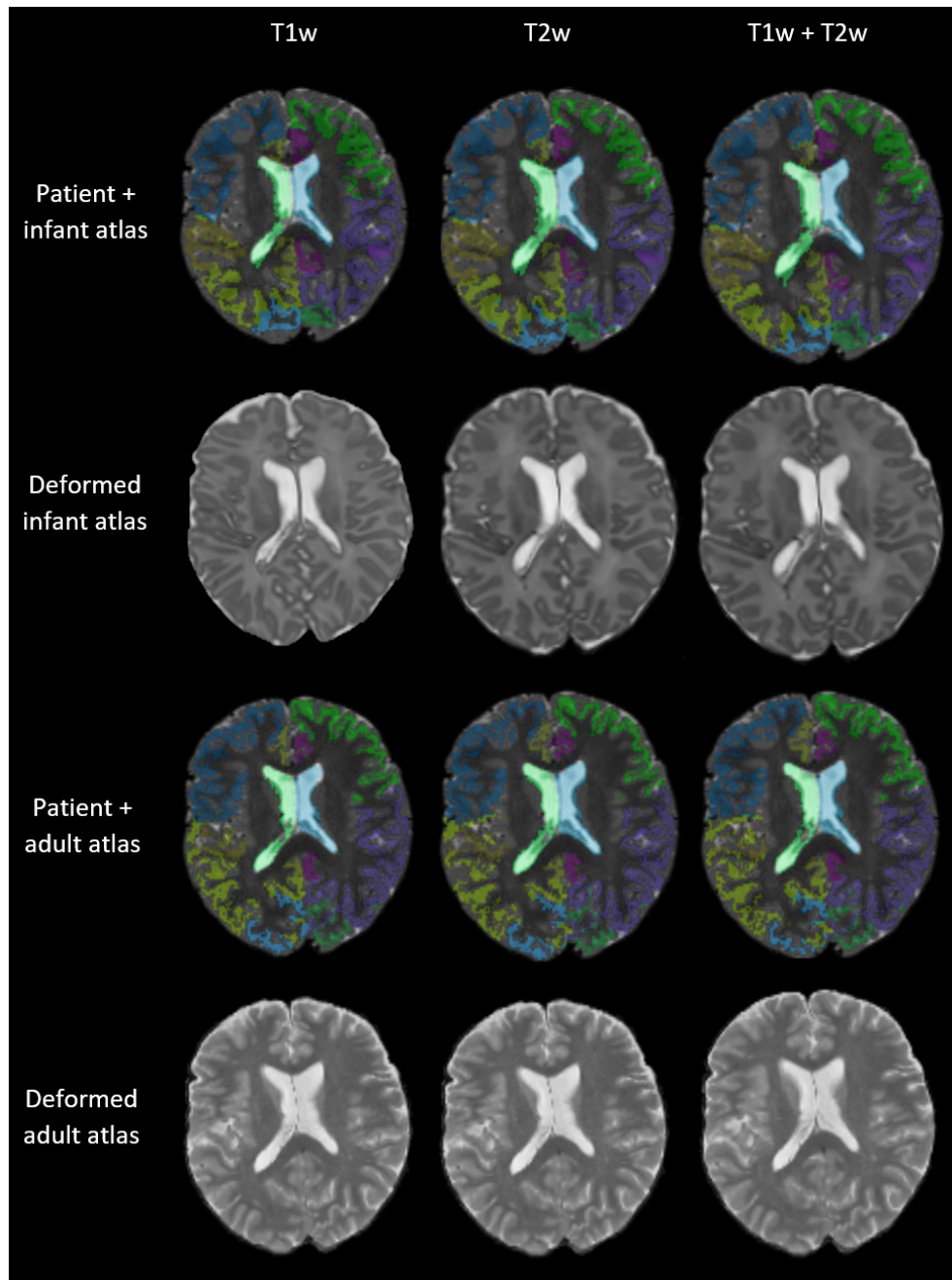


**Fig. 34.** T2w images of infant and adult atlases registered to a child with craniosynostosis using VoxelMorph. Both the deformed atlas scans and patient images with an overlay of the deformed brain regions are shown separately for registration using T1w images, T2w images and both T1w and T2w images. The brain pattern of this child is relatively old and normal looking.

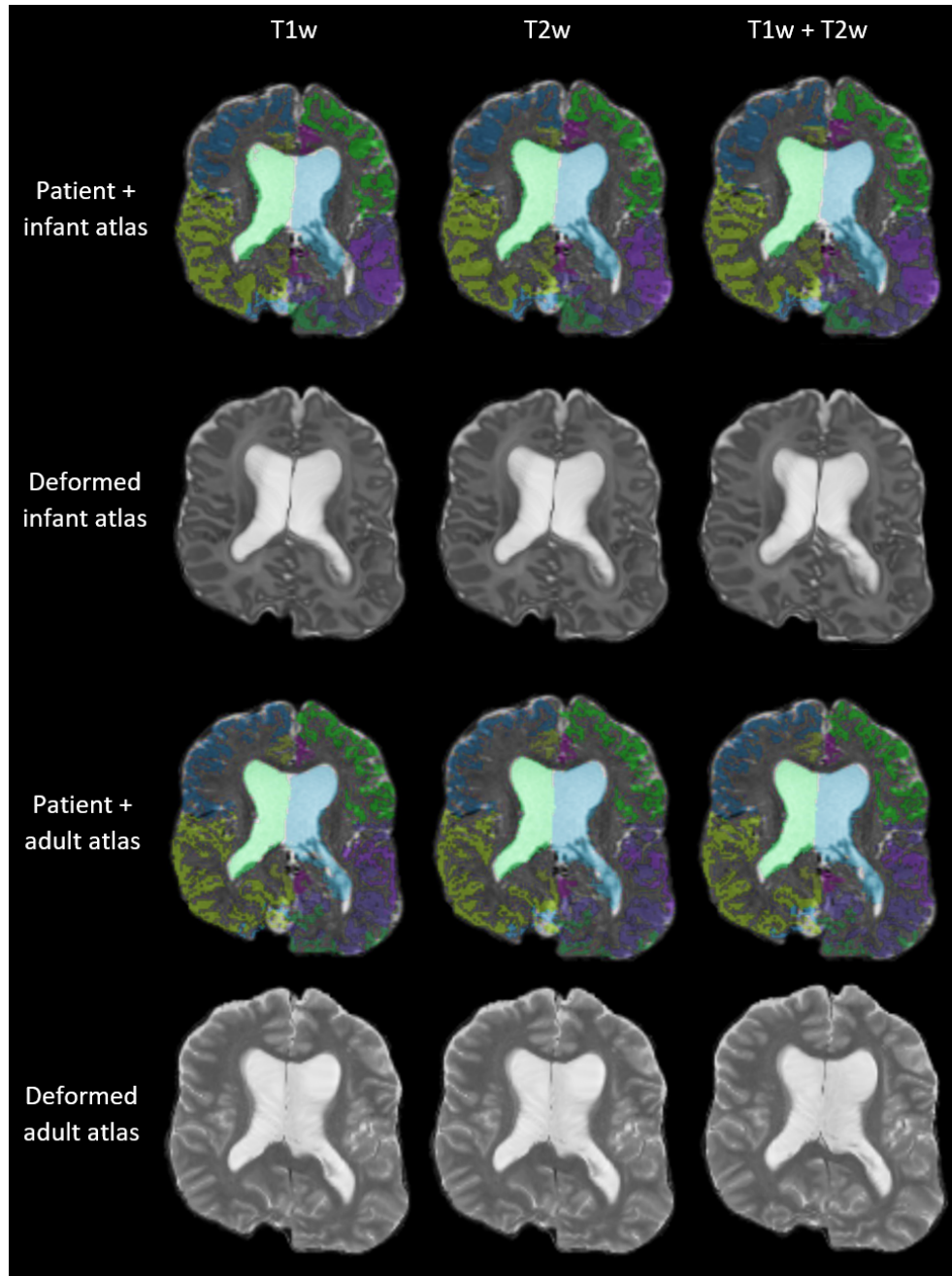


**Fig. 35.** T2w images of infant and adult atlases registered to a child with craniosynostosis using VoxelMorph. Both the deformed atlas scans and patient images with an overlay of the deformed brain regions are shown separately for registration using T1w images, T2w images and both T1w and T2w images. The brain pattern of this child is relatively old and abnormal looking.